J. Fluid Mech. (2013), *vol.* 735, *pp.* 249–287. © Cambridge University Press 2013
doi:10.1017/jfm.2013.502

Weakly nonlinear instability of planar viscous sheets

Lijun Yang†, Chen Wang, Qingfei Fu, Minglong Du and Mingxi Tong

School of Astronautics, Beijing University of Aeronautics and Astronautics, Beijing, 100191, China

(Received 13 September 2012; revised 24 July 2013; accepted 19 September 2013;
first published online 23 October 2013)

A second-order instability analysis has been performed for sinuous disturbances on two-dimensional planar viscous sheets moving in a stationary gas medium using a perturbation technique. The solutions of second-order interface disturbances have been derived for both temporal instability and spatial instability. It has been found that the second-order interface deformation of the fundamental sinuous wave is varicose or dilational, causing disintegration and resulting in ligaments which are interspaced by half a wavelength. The interface deformation has been presented; the breakup time for temporal instability and breakup length for spatial instability have been calculated. An increase in Weber number and gas-to-liquid density ratio extensively increases both the temporal or spatial growth rate and the second-order initial disturbance amplitude, resulting in a shorter breakup time or length, and a more distorted surface deformation. Under normal conditions, viscosity has a stabilizing effect on the first-order temporal or spatial growth rate, but it plays a dual role in the second-order disturbance amplitude. The overall effect of viscosity is minor and complicated. In the typical condition, in which the Weber number is 400 and the gas-to-liquid density ratio is 0.001, viscosity has a weak stabilizing effect when the Reynolds number is larger than 150 or smaller than 10; when the Reynolds number is between 150 and 10, viscosity has a weak destabilizing effect.

Key words: nonlinear instability, thin films, waves/free-surface flows

1. Introduction

The instability of planar liquid sheets has a wide range of applications, such as spray combustion, agricultural sprays, film coating chemicals, pharmaceutical processing and more. Hence a good understanding of the physical mechanism of the breakup is essential for implementation of the practical systems involved. The intrinsic scientific value of the fluid instability is also of great importance. For these reasons, liquid sheet stability has been studied extensively in various aspects by numerous researchers.

The linear instability of thin liquid sheets was first studied by Squire (1953). He investigated the temporal stability of inviscid sheets for the sinuous mode and concluded that the sheet is unstable only when the Weber number is larger than one. He also studied the case when the wavelength is very long compared to its thickness. From this study he found the wavelength for maximum instability. Hagerty & Shea (1955) showed that for inviscid sheets in a linear analysis, only two modes of interface

† Email address for correspondence: yanglijun@buaa.edu.cn

https://doi.org/10.1017/jfm.2013.502 Published online by Cambridge University Press

deformation can exist, i.e. sinuous (antisymmetric) waves and varicose or dilational (symmetric) waves. They also compared the theoretical predictions with experiments. Lin, Lian & Creighton (1990) studied the convective and absolute instability of liquid sheets by analysing the response to impulse, and concluded that with the ambient gas in the sinuous mode, the sheet is convectively unstable when the Weber number is larger than one; but when the Weber number is smaller than one, the sheet is absolutely unstable, while it is always convectively unstable in the varicose mode. The instability of viscous sheets was first studied by Dombrowski & Johns (1963). A drop-sized equation was derived and compared with experimental values. Lin (1981) investigated the stability of a viscous curtain falling down steadily under the influence of gravity. It was found that only the spatially growing sinuous disturbances whose group velocity points upstream are unstable; the group velocity is in the upstream direction only when the Weber number exceeds $1/2$. Li & Tankin (1991) studied the temporal instability of viscous sheets. It was shown that, for sinuous waves, viscosity reduces instability at large Weber numbers but enhances instability at small Weber numbers. The result of a study by Li (1993) showed that the viscosity also reduces the instability at large Weber numbers but plays a dual role at small Weber numbers. The effect of co-flow ambient gas was investigated by Tammisola *et al.* (2011). Both the theoretical prediction and experimental results showed that increasing the velocity of ambient gas first stabilizes and then destabilizes the sheet; this conclusion offers a method for stabilizing the sheets using co-flow gas streams in paper making. The compressibility of ambient gas was studied by Li & Kelly (1992) for inviscid sheets and Cao & Li (2000) for viscous sheets. It was shown that gas compressibility enhances instability.

The studies cited above employed linear analysis to study the instability; linear analysis predicts the onset of sheet instability and shows whether the sheet is stable or unstable, convectively unstable or absolutely unstable. By comparing the temporal or spatial growth rate, the extent of the instability can also be estimated. The linear theory is relatively mature and has been applied broadly; however, linear analysis cannot predict the detailed evolution of the disturbances and the process leading to the eventual breakup. For planar liquid sheets especially, the most unstable mode is the sinuous mode, but it cannot explain why a sheet breaks up, since the two gas–liquid interfaces remain a constant distance apart during wave growth. Crapper, Dombrowski & Pyott (1975) conducted experiments showing large waves on liquid sheets. The experimental results proved that the linear instability theory is inadequate and they developed a preliminary theory for large-amplitude waves on liquid sheets. Asare, Takahashi & Hoffman (1981) also found deviation between the linear theory and experimental observations for higher forcing frequencies and at larger downstream positions, where the wave amplitude appeared to saturate just before breaking up. Therefore, further mechanism of sheet disintegration requires nonlinear analysis.

For capillary waves on inviscid sheets in a vacuum, an exact nonlinear solution was found by Kinnersley (1976), using the assumption that each streamline within the fluid could be a free surface if the fluid above is removed; this was a generalization of Crapper's (1957) exact solution for capillary waves on fluid of infinite depth. Hogan (1986) studied the exact criteria for the highest capillary waves on liquid sheets and presented the profile for both sinuous and varicose waves. He also revised Kinnersley's (1976) study by providing the correct definition of the phase speed of capillary waves. Their exact solutions are straightforward and accurate. However, because the waves they considered are steady and periodic in space, they are not necessarily the cause of the instability.

https://doi.org/10.1017/jfm.2013.502 Published online by Cambridge University Press

The modulational instability of inviscid sheets in a vacuum was studied by Matsuuchi (1974, 1976). Assuming weak nonlinearity, Matsuuchi (1974) employed the multiple scale expansion method and obtained the third-order solution for both symmetric and antisymmetric waves. His analysis revealed that the wave trains of finite amplitude are modulationally unstable. Matsuuchi (1976) further studied the instability of symmetric waves, in which he neglected the assumption of weak nonlinearity but introduced the long-wave approximation. By calculating the second-order solution numerically, he concluded that the waves are remarkably unstable to a subharmonic disturbance.

An important approach to the weakly nonlinear instability problem is the perturbation method, in which the interface displacement η and the velocity potential ϕ can be expanded in a power series of the small initial amplitude η_0:

$$\eta = \eta_0\eta_1 + \eta_0^2\eta_2 + \eta_0^3\eta_3 + \cdots, \tag{1.1a}$$

$$\phi = \eta_0\phi_1 + \eta_0^2\phi_2 + \eta_0^3\phi_3 + \cdots. \tag{1.1b}$$

Clark & Dombrowski (1972) first studied the second-order temporal instability of sinuous waves on inviscid sheets. It was found that the first harmonic of the linear sinuous mode is dilational, which causes the thinning and subsequent rupture of sheets. They used the solution to calculate the breakup length of an attenuating sheet and theoretical predictions were compared with experiments. Jazayeri & Li (2000) extended the perturbation of inviscid sheet instability analysis to third order and found that the second harmonic of a sinuous wave is again sinuous, making the interface more distorted. The effects of various parameters have been discussed and the interface deformations for temporal and spatial mode have been derived. Lee (2002) made a third-order analysis of the instability of a planar sheet stressed at the surface by an electric field. The surface deformation and breakup time have been derived.

Mehring & Sirignano (1999) investigated the capillary wave distortion and disintegration of inviscid sheets. The two-dimensional problem was reduced to a one-dimensional problem by means of the long-wave asymptotic. A second-order exact solution for surface displacement was derived for both sinuous and dilational waves. Comparison with fully two-dimensional nonlinear simulations shows that this one-dimension approach provides representative nonlinear sheet dynamics for both sinuous and dilational disturbances. A similar method was used by Yoshinaga & Kan (2006) to study the breakup of a falling liquid sheet caused by amplified modulational waves. Their results showed that only the sinuous mode is amplified propagating downstream, from which the varicose mode is additionally induced. The numerical simulation agrees well with the weakly nonlinear analysis.

The long-wave asymptotic has also been broadly applied to the instability of thin free liquid sheets or films caused by temperature difference or van der Waals forces. In these studies, the viscosity of liquid has been included. Yoshinaga & Uchiyama (2001) and Yoshinaga & Yoshida (2003) studied the behaviour of a viscous sheet in a vacuum subject to a temperature difference between two surfaces. The surface tension and viscosity were assumed to be a linear decreasing function of the temperature, causing the thermocapillary effect. Results showed that the sheet becomes unstable when the temperature difference is above a certain critical value, and temperature dependence of viscosity enhances instability. Prévost & Gallez (1986), Erneux & Davis (1993), Sharma *et al.* (1995) and Vaynblat, Lister & Witelski (2001) studied a free viscous film subject to van der Waals attractions. Results showed that the van der Waals forces lead to the rupture of the liquid film and the nonlinear effect contributes to

https://doi.org/10.1017/jfm.2013.502 Published online by Cambridge University Press

the acceleration of the rupture phenomenon. The effect of surfactant on the nonlinear rupture of liquid films has been examined by De Wit (1986), Hwang, Chen & Shen (1996) and Lin, Hwang & Uen (2000). Their studies showed that the surfactant has a stabilizing effect and the liquid film with insoluble surfactant is more stable than that with soluble surfactant.

Many authors have used numerical simulations, without long-wave approximation, to study the nonlinear instability of sheets. Rangel & Sirignano (1991) studied the nonlinear Kelvin–Helmholtz instability of inviscid sheets using computational simulation. Results showed that the sinuous mode can exist when the density ratio is of the order of 1. The sinuous mode may result in ligaments which are interspaced by half a wavelength. The varicose mode grows monotonically and may result in ligaments interspaced by one wavelength. Tharakan, Ramamurthi & Balakrishnan (2002) investigated the breakup of inviscid sheets in ambient air. Conservation equations were derived using a control volume method and solved using MacCormack's predictor–corrector scheme. The nonlinear breakup of sheets due to antisymmetric disturbance has been shown. Kan & Yoshinaga (2007) studied the nonlinear instability of a planar liquid sheet with surrounding fluids between two parallel plane solid walls by means of the discrete vortex method. Numerical results showed that the walls enhance nonlinearity, causing deformation and distortion of the sheet.

The previous nonlinear instability analyses of viscous sheets or films (Prévost & Gallez 1986; Erneux & Davis 1993; De Wit, Gallez & Christov 1994; Sharma *et al.* 1995; Hwang *et al.* 1996; Lin *et al.* 2000; Vaynblat *et al.* 2001; Yoshinaga & Uchiyama 2001; Yoshinaga & Yoshida 2003) all used the long-wave approximation and the ambient gas was neglected. In this paper such simplification is removed, because in many practical situations the unstable waves on liquid sheets are not long waves, and the ambient gas plays a vital role in sheet instability. We use a perturbation method similar to the inviscid analysis of Clark & Dombrowski (1972) and Jazayeri & Li (2000) and add the effect of viscosity. By solving the inhomogeneous equations, the second-order solution for surface displacement has been derived and the wave deformation showing the instability has been computed. We also give a detailed study of the effect of Reynolds number to show the role played by viscosity. Here the focus is on the extent of the instability. It can be seen that, although the sheets are all unstable in the situations discussed, their behaviour varies considerably according to the given parameters.

2. Governing equations

A two-dimensional incompressible liquid sheet with a uniform thickness $2a$, density ρ_l, surface tension σ and viscosity μ (schematically shown in figure 1) is considered. For the basic flow, the liquid sheet moves at a uniform velocity of U through a stationary inviscid gas medium of density ρ_g. The gas is assumed to be incompressible. The gravitational effect is neglected because the sheet moves at a relatively high velocity. The coordinates are chosen so that the x-axis is parallel to the direction of the liquid sheet flow, and the y-axis is normal to the liquid sheet with its origin located at the middle plane of the liquid sheet.

When the sheet is disturbed, both interfaces have a displacement and the new location of the two interfaces becomes $y^* = a + \eta_1^*(x, t)$ and $y^* = -a + \eta_2^*(x, t)$. The symbol '*' denotes that the variable is dimensional. Correspondingly, the entire flow field is disturbed and all the parameters acquire a deviation from the base flow. To

https://doi.org/10.1017/jfm.2013.502 Published online by Cambridge University Press

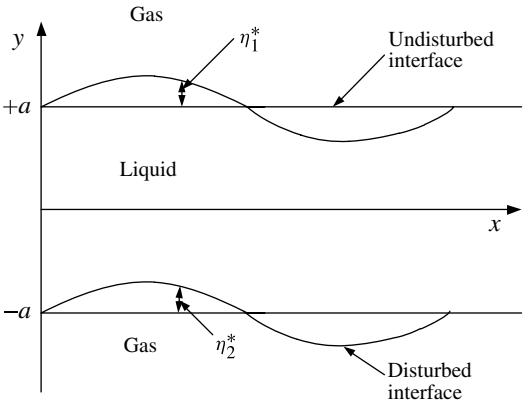


FIGURE 1. Schematic diagram of a moving liquid sheet.

simplify the analysis and make the result more universal, all physical parameters are non-dimensionalized. The length, time and density are scaled with sheet thickness a, convection time a/U and liquid density ρ_l. Pressure is scaled with $\rho_l U^2$. The non-dimensional Reynolds number, liquid Weber number and gas-to-liquid density ratio used in the governing equations are defined as $Re = \rho_l U a/\mu$, $We = \rho_l U^2 a/\sigma$ and $\rho = \rho_g/\rho_l$ respectively.

For the liquid phase, the non-dimensional disturbance velocities in the x and y directions are u and v, and the non-dimensional liquid pressure is p. Because the gas considered is inviscid, in the gas phase it is assumed that flow is initially irrotational, so it has a non-dimensional velocity potential ϕ_{gj}, where $j = 1$ represents the gas above the liquid sheet and $j = 2$ represents the gas below. The gas phase pressure is defined as p_{gj}. The non-dimensionalized interface deformations are set to be η_j, where $j = 1$ corresponds to the upper interface and $j = 2$ to the lower interface.

The liquid phase must satisfy the mass conservation equation:

$$\frac{\partial u}{\partial x} + \frac{\partial v}{\partial y} = 0 \quad \text{for } -1 + \eta_2 < y < 1 + \eta_1. \tag{2.1}$$

The equations of momentum for viscous liquid are given by

$$\frac{\partial u}{\partial t} + (1+u)\frac{\partial u}{\partial x} + v\frac{\partial u}{\partial y} = -\frac{\partial p}{\partial x} + \frac{1}{Re}\left(\frac{\partial^2 u}{\partial x^2} + \frac{\partial^2 u}{\partial y^2}\right)$$
$$\text{for } -1 + \eta_2 < y < 1 + \eta_1, \tag{2.2}$$
$$\frac{\partial v}{\partial t} + (1+u)\frac{\partial v}{\partial x} + v\frac{\partial v}{\partial y} = -\frac{\partial p}{\partial y} + \frac{1}{Re}\left(\frac{\partial^2 v}{\partial x^2} + \frac{\partial^2 v}{\partial y^2}\right)$$
$$\text{for } -1 + \eta_2 < y < 1 + \eta_1. \tag{2.3}$$

Note that '1' in the term '$1 + u$' represents the basic x direction uniform flow.

The kinematic boundary condition requires

$$v = \frac{\partial \eta_j}{\partial t} + (1+u)\frac{\partial \eta_j}{\partial x} \quad \text{at } y = (-1)^{j+1} + \eta_j. \tag{2.4}$$

https://doi.org/10.1017/jfm.2013.502 Published online by Cambridge University Press

As the gas phase is inviscid, the liquid shear stress at the interface should vanish:

$$(\boldsymbol{n}_j \cdot \boldsymbol{\tau}) \times \boldsymbol{n}_j = \boldsymbol{0} \quad \text{at } y = (-1)^{j+1} + \eta_j, \tag{2.5}$$

where $\boldsymbol{n}_j$ is the interface unit normal vector and $\boldsymbol{\tau}$ is the extra stress tensor:

$$\boldsymbol{n}_j = \frac{\nabla F_j}{|\nabla F_j|}, \quad F_j = y - \eta_j, \quad \boldsymbol{\tau} = \frac{1}{Re}\left[\nabla \boldsymbol{v} + (\nabla \boldsymbol{v})^{\mathrm{T}}\right], \quad \boldsymbol{v} = (1+u, v, 0). \tag{2.6}$$

For the gas phase, the mass conservation equation is

$$\frac{\partial^2 \phi_{gj}}{\partial x^2} + \frac{\partial^2 \phi_{gj}}{\partial y^2} = 0, \quad j = 1, 2 \text{ for } y > 1 + \eta_1, y < -1 + \eta_2. \tag{2.7}$$

The pressure of the gas phase can be obtained from the Cauchy–Lagrange integration:

$$p_{gj} = -\rho \left[\frac{\partial \phi_{gj}}{\partial t} + \frac{1}{2}\left(\frac{\partial \phi_{gj}}{\partial x}\right)^2 + \frac{1}{2}\left(\frac{\partial \phi_{gj}}{\partial y}\right)^2 \right],$$
$$j = 1, 2 \text{ for } y > 1 + \eta_1, y < -1 + \eta_2. \tag{2.8}$$

The kinematic boundary condition for the gas phase is given by

$$\frac{\partial \phi_{gj}}{\partial y} = \frac{\partial \eta_j}{\partial t} + \frac{\partial \phi_{gj}}{\partial x}\frac{\partial \eta_j}{\partial x} \quad \text{at } y = (-1)^{j+1} + \eta_j. \tag{2.9}$$

The normal stress at the interface should be continuous, so the dynamic boundary condition requires

$$-p + \left(\boldsymbol{n}_j \cdot \boldsymbol{\tau}\right) \cdot \boldsymbol{n}_j + (-1)^{j+1}\frac{1}{We}(\nabla \cdot \boldsymbol{n}_j) + p_{gj} = 0 \quad \text{at } y = (-1)^{j+1} + \eta_j. \tag{2.10}$$

Equations (2.1) to (2.10) are all the governing equations and boundary conditions needed to describe the flow field. It is assumed that this is a weakly nonlinear problem and all the disturbance parameters can be expanded into a perturbation form:

$$(u, v, p, \phi_{gj}, p_{gj}) = (u_1, v_1, p_1, \phi_{gj1}, p_{gj1})\eta_0 + (u_2, v_2, p_2, \phi_{gj2}, p_{gj2})\eta_0^2 + \cdots. \tag{2.11}$$

In particular, this is also valid for the interface deformation

$$\eta_j = \eta_{j1}\eta_0 + \eta_{j2}\eta_0^2 + \cdots, \tag{2.12}$$

where η_0 is the small parameter in the perturbation expansion and here it is defined as the initial disturbance. In the present study, the perturbation expansion proceeds to second order. The third or higher orders are neglected; they are left to be studied in further work.

For the equations on the disturbed boundaries, it is assumed that the parameters on the disturbed boundaries can be expressed by a Taylor series, using their values and derivatives on the undisturbed boundaries:

$$\left(\frac{\partial \phi_{gj}}{\partial x}, \frac{\partial \phi_{gj}}{\partial t}, u, v, p, p_{gj}\right)\Bigg|_{y=(-1)^{j+1}+\eta_j} = \left(\frac{\partial \phi_{gj}}{\partial x}, \frac{\partial \phi_{gj}}{\partial t}, u, v, p, p_{gj}\right)\Bigg|_{y=(-1)^{j+1}}$$
$$+ \frac{\partial}{\partial y}\left(\frac{\partial \phi_{gj}}{\partial x}, \frac{\partial \phi_{gj}}{\partial t}, u, v, p, p_{gj}\right)\Bigg|_{y=(-1)^{j+1}} \eta_j + \cdots. \tag{2.13}$$

https://doi.org/10.1017/jfm.2013.502 Published online by Cambridge University Press

Substituting (2.11)–(2.13) into (2.1)–(2.10), collecting the terms with coefficients η_0 and η_0^2, the first-order and second-order equations can be obtained. The first-order equations are given by

$$\frac{\partial u_1}{\partial x}+\frac{\partial v_1}{\partial y}=0 \quad \text{for } -1<y<1, \tag{2.14}$$

$$\frac{\partial u_1}{\partial t}+\frac{\partial u_1}{\partial x}=-\frac{\partial p_1}{\partial x}+\frac{1}{Re}\left(\frac{\partial^2 u_1}{\partial x^2}+\frac{\partial^2 u_1}{\partial y^2}\right) \quad \text{for } -1<y<1, \tag{2.15}$$

$$\frac{\partial v_1}{\partial t}+\frac{\partial v_1}{\partial x}=-\frac{\partial p_1}{\partial y}+\frac{1}{Re}\left(\frac{\partial^2 v_1}{\partial x^2}+\frac{\partial^2 v_1}{\partial y^2}\right) \quad \text{for } -1<y<1, \tag{2.16}$$

$$v_1=\frac{\partial \eta_{j1}}{\partial t}+\frac{\partial \eta_{j1}}{\partial x} \quad \text{at } y=(-1)^{j+1}, \tag{2.17}$$

$$\frac{1}{Re}\left(\frac{\partial u_1}{\partial y}+\frac{\partial v_1}{\partial x}\right)=0 \quad \text{at } y=\pm 1, \tag{2.18}$$

$$\frac{\partial^2 \phi_{gj1}}{\partial x^2}+\frac{\partial^2 \phi_{gj1}}{\partial y^2}=0, \quad j=1,2 \text{ for } y>1, y<-1, \tag{2.19}$$

$$p_{gj1}=-\rho\frac{\partial \phi_{gj1}}{\partial t}, \quad j=1,2 \text{ for } y>1, y<-1, \tag{2.20}$$

$$\frac{\partial \phi_{gj1}}{\partial y}=\frac{\partial \eta_{j1}}{\partial t} \quad \text{at } y=(-1)^{j+1}, \tag{2.21}$$

$$-p_1+\frac{2}{Re}\frac{\partial v_1}{\partial y}+(-1)^j\frac{1}{We}\frac{\partial^2 \eta_{j1}}{\partial x^2}+p_{gj1}=0 \quad \text{at } y=(-1)^{j+1}. \tag{2.22}$$

Correspondingly, the second-order equations are

$$\frac{\partial u_2}{\partial x}+\frac{\partial v_2}{\partial y}=0 \quad \text{for } -1<y<1, \tag{2.23}$$

$$\frac{\partial u_2}{\partial t}+\frac{\partial u_2}{\partial x}+u_1\frac{\partial u_1}{\partial x}+v_1\frac{\partial u_1}{\partial y}=-\frac{\partial p_2}{\partial x}+\frac{1}{Re}\left(\frac{\partial^2 u_2}{\partial x^2}+\frac{\partial^2 u_2}{\partial y^2}\right) \quad \text{for } -1<y<1, \tag{2.24}$$

$$\frac{\partial v_2}{\partial t}+\frac{\partial v_2}{\partial x}+u_1\frac{\partial v_1}{\partial x}+v_1\frac{\partial v_1}{\partial y}=-\frac{\partial p_2}{\partial y}+\frac{1}{Re}\left(\frac{\partial^2 v_2}{\partial x^2}+\frac{\partial^2 v_2}{\partial y^2}\right) \quad \text{for } -1<y<1, \tag{2.25}$$

$$v_2=\frac{\partial \eta_{j2}}{\partial t}+\frac{\partial \eta_{j2}}{\partial x}+u_1\frac{\partial \eta_{j1}}{\partial x}-\eta_{j1}\frac{\partial v_1}{\partial y} \quad \text{at } y=(-1)^{j+1}, \tag{2.26}$$

$$\frac{1}{Re}\left[\frac{\partial u_2}{\partial y}+\frac{\partial v_2}{\partial x}+\eta_{j1}\frac{\partial}{\partial y}\left(\frac{\partial u_1}{\partial y}+\frac{\partial v_1}{\partial x}\right)+2\left(\frac{\partial v_1}{\partial y}-\frac{\partial u_1}{\partial x}\right)\frac{\partial \eta_{j1}}{\partial x}\right]=0 \quad \text{at } y=(-1)^{j+1}, \tag{2.27}$$

$$\frac{\partial^2 \phi_{gj2}}{\partial x^2}+\frac{\partial^2 \phi_{gj2}}{\partial y^2}=0, \quad j=1,2 \text{ for } y>1, y<-1, \tag{2.28}$$

$$p_{gj2}=-\rho\left[\frac{\partial \phi_{gj2}}{\partial t}+\frac{1}{2}\left(\frac{\partial \phi_{gj1}}{\partial x}\right)^2+\frac{1}{2}\left(\frac{\partial \phi_{gj1}}{\partial y}\right)^2\right], \quad j=1,2 \text{ for } y>1, y<-1, \tag{2.29}$$

https://doi.org/10.1017/jfm.2013.502 Published online by Cambridge University Press

$$\frac{\partial \phi_{gj2}}{\partial y} = \frac{\partial \eta_{j2}}{\partial t} + \frac{\partial \phi_{gj1}}{\partial x}\frac{\partial \eta_{j1}}{\partial x} - \eta_{j1}\frac{\partial}{\partial y}\left(\frac{\partial \phi_{gj1}}{\partial y}\right) \quad \text{at } y = (-1)^{j+1}, \tag{2.30}$$

$$-p_2 + \frac{2}{Re}\frac{\partial v_2}{\partial y} + (-1)^j \frac{1}{We}\frac{\partial^2 \eta_{j2}}{\partial x^2} + p_{gj2} - \eta_{j1}\frac{\partial p_1}{\partial y} + \frac{2}{Re}\eta_{j1}\frac{\partial^2 v_1}{\partial y^2} - \frac{2}{Re}\left(\frac{\partial u_1}{\partial y} + \frac{\partial v_1}{\partial x}\right)\frac{\partial \eta_{j1}}{\partial x} + \eta_{j1}\frac{\partial p_{gj1}}{\partial y} = 0 \quad \text{at } y = (-1)^{j+1}. \tag{2.31}$$

It can be seen that the first-order equations (2.14)–(2.22) are linear in x and t, and they are identical to the former linear analyses presented by Lin (1981) and Li & Tankin (1991), so they can be solved using the linear analysis method. In the second-order equations, all the nonlinear terms involved are the first-order solutions which will already have been solved; in this way, the second-order solution can be obtained. The second-order solutions provide more information and make the result more accurate.

3. Mathematical solutions

3.1. *First-order solutions*

The first-order equations are linear in x and t, and therefore they have the normal mode solution

$$(u_1, v_1, p_1, \phi_{gj1}, p_{gj1}, \eta_{j1}) = [\hat{u}_1, \hat{v}_1, \hat{p}_1, \hat{\phi}_{gj1}, \hat{p}_{gj1}, \hat{\eta}_{j1}] \exp[\mathrm{i}(k_1 x - \omega_1 t)] + \text{c.c.}, \tag{3.1}$$

where k_1 and ω_1 are the first-order complex wavenumber and frequency respectively, their real parts k_{1r} and ω_{1r} represent the spatial and temporal oscillation frequency and the imaginary parts k_{1i} and ω_{1i} represent the spatial and temporal exponential growth rate. The symbol '$\hat{}$' indicates the disturbance amplitude which is a function of y only and specially, $\hat{\eta}_{j1}$ is a constant; 'c.c.' in (3.1) represents the complex conjugate.

The linear stability analysis investigated by Hagerty & Shea (1955) has shown that only two modes exist for inviscid sheets, i.e. sinuous (antisymmetric) waves and varicose (symmetric) or dilational waves. Lin (1981), Li & Tankin (1991) and Li (1993) extended the linear analysis to viscous sheets and obtained a similar conclusion. All their studies showed that the sinuous mode dominates for a wide range of parameters, especially in practical situations. More importantly, the waves observed in the experiments conducted by Tammisola *et al.* (2011) are sinuous. Therefore, in the present study, it is assumed that the linear part (i.e. the first-order solutions) is sinuous.

For the sinuous mode, the upper and lower interface disturbances are the same:

$$(\eta_{j1})_{j=1} = (\eta_{j1})_{j=2}, \quad (\hat{\eta}_{j1})_{j=1} = (\hat{\eta}_{j1})_{j=2}. \tag{3.2}$$

The first-order solutions of the liquid phase for the sinuous mode can be solved to give

$$\hat{u}_1 = \frac{\mathrm{i}l_1}{k_1}B_1 \sinh l_1 y + \mathrm{i}D_1 \sinh k_1 y, \quad \hat{v}_1 = B_1 \cosh l_1 y + D_1 \cosh k_1 y, \tag{3.3}$$

$$\hat{p}_1 = \frac{\omega_1 - k_1}{k_1}\mathrm{i}D_1 \sinh k_1 y, \tag{3.4}$$

$$B_1 = -\frac{2k_1^2}{Re \cosh l_1}\hat{\eta}_{j1}, \quad D_1 = \frac{k_1^2 + l_1^2}{Re \cosh k_1}\hat{\eta}_{j1}, \quad l_1^2 = k_1^2 + \mathrm{i}Re(k_1 - \omega_1). \tag{3.5}$$

https://doi.org/10.1017/jfm.2013.502 Published online by Cambridge University Press

For the gas phase, the solutions are

$$\hat{\phi}_{gj1} = (-1)^{j+1}\hat{\eta}_{j1}\frac{\mathrm{i}\omega_1}{k_1}\exp[k_1 + (-1)^j k_1 y] \tag{3.6}$$

$$\hat{p}_{gj1} = (-1)^j \hat{\eta}_{j1}\rho\frac{\omega_1^2}{k_1}\exp[k_1 + (-1)^j k_1 y], \tag{3.7}$$

where k_1 and ω_1 should satisfy the first-order dispersion relation for the sinuous mode,

$$D_{sin}(\omega_1, k_1) = 0, \tag{3.8}$$

where $D_{sin}(\omega, k)$ is defined by

$$D_{sin}(\omega, k) = -\rho\omega^2 + \frac{k^3}{We} + \frac{(l^2 + k^2)^2}{Re^2}\tanh k - \left(\frac{2}{Re}\right)^2 lk^3 \tanh l, \tag{3.9}$$

$$l^2 = k^2 + \mathrm{i}Re(k - \omega). \tag{3.10}$$

Equation (3.10) is identical to the linear analysis presented by Lin (1981), Li & Tankin (1991) and Li (1993). For inviscid sheets, $Re \to \infty$, (3.10) reduces to that presented by Squire (1953):

$$[D_{sin}(\omega, k)]_{Re\to\infty} = -\rho\omega^2 + \frac{k^3}{We} - (\omega - k)^2 \tanh k. \tag{3.11}$$

The dispersion character equation for the other, varicose, mode is (Lin 1981; Li 1993)

$$D_{var}(\omega, k) = -\rho\omega^2 + \frac{k^3}{We} + \frac{(l^2 + k^2)^2}{Re^2}\coth k - \left(\frac{2}{Re}\right)^2 lk^3 \coth l, \tag{3.12}$$

$$l^2 = k^2 + \mathrm{i}Re(k - \omega) \tag{3.13}$$

and for inviscid sheets (Hagerty & Shea 1955),

$$[D_{var}(\omega, k)]_{Re\to\infty} = -\rho\omega^2 + \frac{k^3}{We} - (\omega - k)^2 \coth k. \tag{3.14}$$

They will be used in the subsequent discussion.

The first-order linear solutions are standard and well known, and more details can be found in the cited literature. The linear analysis predicts the onset of sheet instability and focuses mainly on the dispersion relation. By analysing the response to the impulse disturbance, Lin (1981) concluded that the sinuous wave of the sheet is convectively unstable when the Weber number is larger than one and absolutely unstable when the Weber number is smaller than one, with the ambient gas. Using Fourier inverse transformation, the response of any disturbance can be derived. In the present study, the focus is on only two of the most typical forms of instability, i.e. temporal instability and spatial instability.

3.2. *Second-order solutions for temporal instability*

In temporal instability, it is assumed that liquid sheet is infinite, a small disturbance, which is periodic in space, is imposed on the sheet and the disturbance increases exponentially at the same time rate everywhere. The temporal revolution of the sheet indicates the sheet's instability. Therefore the wavenumber k_1 is real and the temporal frequency ω_1 is complex; the imaginary part ω_{1i} represents the temporal exponential growth rate and causes the instability. According to the discussions above,

https://doi.org/10.1017/jfm.2013.502 Published online by Cambridge University Press

it is assumed that there is a sinuous disturbance at the beginning. The initial condition is given by

$$(\eta_j)_{j=1}|_{t=0} = (\eta_j)_{j=2}|_{t=0} = \eta_0 \cos k_1 x = \tfrac{1}{2}\eta_0 \exp(\mathrm{i}k_1 x) + \text{c.c.}, \tag{3.15}$$

where η_0 is the initial disturbance amplitude.

The second-order solutions are based on the first-order solutions. According to the forms of first-order solutions expressed in (3.1), noticing that k_1 is real and ω_1 is complex, the first-order nonlinear terms involved in second-order equations (2.24)–(2.27) and (2.31) can be expressed in the following forms:

$$u_1\frac{\partial u_1}{\partial x} + v_1\frac{\partial u_1}{\partial y} = \hat{f}_u \exp[2\mathrm{i}(k_1 x - \omega_1 t)] + \hat{g}_u \exp(2\omega_{1i} t) + \text{c.c.}, \tag{3.16}$$

$$u_1\frac{\partial v_1}{\partial x} + v_1\frac{\partial v_1}{\partial y} = \hat{f}_v \exp[2\mathrm{i}(k_1 x - \omega_1 t)] + \hat{g}_v \exp(2\omega_{1i} t) + \text{c.c.}, \tag{3.17}$$

$$u_1\frac{\partial \eta_{j1}}{\partial x} - \eta_{j1}\frac{\partial v_1}{\partial y} = \hat{f}_\eta \exp[2\mathrm{i}(k_1 x - \omega_1 t)] + \hat{g}_\eta \exp(2\omega_{1i} t) + \text{c.c.}, \tag{3.18}$$

$$\begin{aligned}&\eta_{j1}\frac{\partial}{\partial y}\left(\frac{\partial u_1}{\partial y} + \frac{\partial v_1}{\partial x}\right) + 2\left(\frac{\partial v_1}{\partial y} - \frac{\partial u_1}{\partial x}\right)\frac{\partial \eta_{j1}}{\partial x}\\ &\quad = \hat{f}_\mu \exp[2\mathrm{i}(k_1 x - \omega_1 t)] + \hat{g}_\mu \exp(2\omega_{1i} t) + \text{c.c.},\end{aligned} \tag{3.19}$$

$$\begin{aligned}&-\eta_{j1}\frac{\partial p_1}{\partial y} + \frac{2}{Re}\eta_{j1}\frac{\partial^2 v_1}{\partial y^2} - \frac{2}{Re}\left(\frac{\partial u_1}{\partial y} + \frac{\partial v_1}{\partial x}\right)\frac{\partial \eta_{j1}}{\partial x} + \eta_{j1}\frac{\partial p_{gj1}}{\partial y}\\ &\quad = \hat{f}_d \exp[2\mathrm{i}(k_1 x - \omega_1 t)] + \hat{g}_d \exp(2\omega_{1i} t) + \text{c.c.},\end{aligned} \tag{3.20}$$

where $\hat{f}_u$, $\hat{f}_v$, $\hat{f}_\eta$, $\hat{f}_\mu$, $\hat{f}_d$, $\hat{g}_u$, $\hat{g}_v$, $\hat{g}_\eta$, $\hat{g}_\mu$ and $\hat{g}_d$ are functions of y only. The expressions for $\hat{f}_u$, $\hat{f}_v$, $\hat{f}_\eta$, $\hat{f}_\mu$ and $\hat{f}_d$ are given in appendix A; the expressions for $\hat{g}_u$, $\hat{g}_v$, $\hat{g}_\eta$, $\hat{g}_\mu$ and $\hat{g}_d$ are not noted because they are not used to describe the interface disturbance amplitude.

So according to the forms of the first-order nonlinear terms expressed in (3.16)–(3.20), the second-order solutions are assumed to be

$$\begin{aligned}(u_2, v_2, p_2, \phi_{gj2}, p_{gj2}, \eta_{j2}) = {}& [\hat{u}_{21}, \hat{v}_{21}, \hat{p}_{21}, \hat{\phi}_{gj21}, \hat{p}_{gj21}, \hat{\eta}_{j21}] \exp[2\mathrm{i}(k_1 x - \omega_1 t)]\\ &+ [\hat{u}_{22}, \hat{v}_{22}, \hat{p}_{22}, \hat{\phi}_{gj22}, \hat{p}_{gj22}, \hat{\eta}_{j22}] \exp(2\omega_{1i} t)\\ &+ [\hat{u}_{23}, \hat{v}_{23}, \hat{p}_{23}, \hat{\phi}_{gj23}, \hat{p}_{gj23}, \hat{\eta}_{j23}] \exp[\mathrm{i}(2k_1 x - \omega_2 t)]\\ &+ [\hat{u}_{24}, \hat{v}_{24}, \hat{p}_{24}, \hat{\phi}_{gj24}, \hat{p}_{gj24}, \hat{\eta}_{j24}] \exp(-\mathrm{i}\omega_2' t) + \text{c.c.}\end{aligned} \tag{3.21}$$

The first and second terms in (3.21), with subscript 21 and 22, are generated from the first-order solutions and they have the same wavenumbers and frequencies as those in (3.16) to (3.20). They represent the energy transfer from the fundamental first order to second order. The third and fourth terms with subscript 23 and 24 represent the inherent second-order instability and they correspond to homogeneous equations. ω_2 and ω_2' are the second-order frequencies corresponding to wavenumber $2k_1$ and 0. The wavenumbers are chosen to be the same as the terms with subscript 21 and 22 in order to satisfy the initial condition (3.15).

The second-order disturbances with subscript 21 in (3.21) will be solved first. Combining (2.23), (2.24) and (2.25) yields

$$\frac{\partial^2 p_2}{\partial x^2} + \frac{\partial^2 p_2}{\partial y^2} = -\frac{\partial}{\partial x}\left(u_1\frac{\partial u_1}{\partial x} + v_1\frac{\partial u_1}{\partial y}\right) - \frac{\partial}{\partial y}\left(u_1\frac{\partial v_1}{\partial x} + v_1\frac{\partial v_1}{\partial y}\right). \tag{3.22}$$

https://doi.org/10.1017/jfm.2013.502 Published online by Cambridge University Press

Substituting (3.16), (3.17) and (3.21) into (3.22), collecting the terms with coefficient $\exp[2\mathrm{i}(k_1x-\omega_1t)]$ yields

$$\frac{\mathrm{d}^2\hat{p}_{21}}{\mathrm{d}y^2}-4k_1^2\hat{p}_{21}=-\left(2\mathrm{i}k_1\hat{f}_u+\frac{\mathrm{d}\hat{f}_v}{\mathrm{d}y}\right)=\hat{f}_p, \tag{3.23}$$

where $\hat{f}_p$ is a new variable defined in (3.23). Solving (3.23) yields

$$\hat{p}_{21}=C_p\exp(2k_1y)+D_p\exp(-2k_1y)+\hat{h}_p, \tag{3.24}$$

where C_p and D_p are integration constants to be found and $\hat{h}_p$ is the particular solution of (3.23), satisfying the inhomogeneous term $\hat{f}_p$. The expressions for $\hat{f}_p$ and $\hat{h}_p$ are given in appendix A; $\hat{f}_p$ consists of constants and hyperbolic functions, so according to (3.23), $\hat{h}_p$ also consists of constants and hyperbolic functions and has the same parity as $\hat{f}_p$. The symbol $\hat{h}_p$ is used here to represent the particular solution so that the calculation process can be greatly simplified. This method is also used in the following calculation process.

Substituting (3.16), (3.21) and (3.24) into (2.24) yields

$$\frac{\mathrm{d}^2\hat{u}_{21}}{\mathrm{d}y^2}-l_{21}^2\hat{u}_{21}=Re\{2\mathrm{i}k_1[C_p\exp(2k_1y)+D_p\exp(-2k_1y)+\hat{h}_p]+\hat{f}_u\}, \tag{3.25}$$

where

$$l_{21}^2=4k_1^2+2\mathrm{i}Re(k_1-\omega_1). \tag{3.26}$$

Substituting (3.17), (3.21) and (3.24) into (2.25) yields

$$\frac{\mathrm{d}^2\hat{v}_{21}}{\mathrm{d}y^2}-l_{21}^2\hat{v}_{21}=Re\left\{2k_1\left[C_p\exp(2k_1y)-D_p\exp(-2k_1y)\right]+\frac{\mathrm{d}\hat{h}_p}{\mathrm{d}y}+\hat{f}_v\right\}. \tag{3.27}$$

The solutions of (3.25) and (3.27) are

$$\begin{aligned}\hat{u}_{21}&=C_u\exp(l_{21}y)+D_u\exp(-l_{21}y)\\&\quad+Re\frac{2\mathrm{i}k_1}{4k_1^2-l_{21}^2}\left[C_p\exp(2k_1y)+D_p\exp(-2k_1y)\right]+\hat{h}_u,\end{aligned} \tag{3.28}$$

$$\begin{aligned}\hat{v}_{21}&=C_v\exp(l_{21}y)+D_v\exp(-l_{21}y)\\&\quad+Re\frac{2k_1}{4k_1^2-l_{21}^2}[C_p\exp(2k_1y)-D_p\exp(-2k_1y)]+\hat{h}_v,\end{aligned} \tag{3.29}$$

where $\hat{h}_u$ is the particular solution of

$$\frac{\mathrm{d}^2\hat{u}_{21}}{\mathrm{d}y^2}-l_{21}^2\hat{u}_{21}=Re(2\mathrm{i}k_1\hat{h}_p+\hat{f}_u) \tag{3.30}$$

and $\hat{h}_v$ is the particular solution of

$$\frac{\mathrm{d}^2\hat{v}_{21}}{\mathrm{d}y^2}-l_{21}^2\hat{v}_{21}=Re\left(\frac{\mathrm{d}\hat{h}_p}{\mathrm{d}y}+\hat{f}_v\right). \tag{3.31}$$

The expressions for $\hat{f}_u$, $\hat{f}_v$, $\hat{h}_u$ and $\hat{h}_v$ are given in appendix A.

https://doi.org/10.1017/jfm.2013.502 Published online by Cambridge University Press

Substituting (3.21) into mass conservation equation (2.23), collecting the terms with coefficient $\exp[2\mathrm{i}(k_1x-\omega_1t)]$ yields

$$\hat{u}_{21}=\frac{\mathrm{i}}{2k_1}\frac{\mathrm{d}\hat{v}_{21}}{\mathrm{d}y}. \tag{3.32}$$

Inserting (3.28), (3.29) into the conservation equation (3.32) yields

$$C_u=\frac{\mathrm{i}l_{21}}{2k_1}C_v,\quad D_u=-\frac{\mathrm{i}l_{21}}{2k_1}D_v. \tag{3.33}$$

Note that $\hat{h}_u$ and $\hat{h}_v$ have a relation shown as (A 7) in appendix A and satisfy the mass conservation equation (3.32).

For the gas phase, substituting (3.21) into (2.28), collecting the terms with coefficient $\exp[2\mathrm{i}(k_1x-\omega_1t)]$, and noticing the disturbance should not be infinite at $y\to\infty$, one arrives at

$$\hat{\phi}_{gj21}=C_{gj}\exp\left[(-1)^j2k_1y\right]. \tag{3.34}$$

Inserting (3.34), (3.6) and (3.21) into kinematic boundary condition (2.30), we find

$$C_{gj}=\left[\frac{(-1)^{j+1}\hat{\eta}_{j21}}{k_1}+\hat{\eta}_{j1}^2\right]\mathrm{i}\omega_1\exp(2k_1). \tag{3.35}$$

Substituting (3.34), (3.35), (3.6) and (3.21) into (2.29), the second-order gas phase pressure yields

$$\hat{p}_{gj21}=\frac{2\omega_1^2\rho}{k_1}\left[(-1)^j\hat{\eta}_{j21}-k_1\hat{\eta}_{j1}^2\right]\exp\left[2k_1+(-1)^j2k_1y\right]. \tag{3.36}$$

Using the expression in (3.18), (3.19), (3.20) and (3.21), the boundary condition (2.26), (2.27), (2.31) for terms with coefficient $\exp[2\mathrm{i}(k_1x-\omega_1t)]$ yields

$$\hat{v}_{21}=2\mathrm{i}(k_1-\omega_1)\hat{\eta}_{j21}+\hat{f}_\eta\quad\text{at } y=(-1)^{j+1}, \tag{3.37}$$

$$\frac{\mathrm{d}\hat{u}_{21}}{\mathrm{d}y}+2\mathrm{i}k_1\,\hat{v}_{21}+\hat{f}_\mu=0\quad\text{at } y=\pm1, \tag{3.38}$$

$$-\hat{p}_{21}+\frac{2}{Re}\frac{\mathrm{d}\hat{v}_{21}}{\mathrm{d}y}+\hat{p}_{gj21}+\frac{1}{We}(-1)^{j+1}4k_1^2\hat{\eta}_{j21}+\hat{f}_d=0\quad\text{at } y=(-1)^{j+1}. \tag{3.39}$$

The expressions for $\hat{f}_\eta$, $\hat{f}_\mu$ and $\hat{f}_d$ are given in appendix A. Substituting (3.24), (3.29), (3.32) and (3.36) into boundary conditions (3.37), (3.38) and (3.39), we obtain six linear algebra equations of six unknown constants C_v, D_v, C_p, D_p, and $\hat{\eta}_{j21}(j=1,2)$. It can be seen that the coefficient matrix of C_v, D_v, C_p, D_p, and $\hat{\eta}_{j21}(j=1,2)$ is the same as the first-order linear analysis if $2k_1$ and $2\omega_1$ are replaced with k_1 and ω_1 respectively. Therefore, according to linear analysis, the coefficient matrix of C_v, D_v, C_p, D_p, and $\hat{\eta}_{j21}(j=1,2)$ is singular only when the corresponding dispersion relation is satisfied:

$$D_{sin}(2\omega_1,2k_1)=0\quad\text{or}\quad D_{var}(2\omega_1,2k_1)=0. \tag{3.40}$$

As k_1 and ω_1 have already satisfied $D_{sin}(\omega_1,k_1)=0$, (3.40) does not hold. So the coefficient matrix of C_v, D_v, C_p, D_p, and $\hat{\eta}_{j21}(j=1,2)$ is non-singular. According to Cramer's rule in linear algebra, the solution exists and is single.

Hence $\hat{\eta}_{j21}(j=1,2)$ can be directly solved, but the process can be simplified in the following way. According to (3.5) and (3.7), $\hat{p}_{gj1}$ and $\hat{u}_1$ are odd and $\hat{v}_1$ is even, so it

https://doi.org/10.1017/jfm.2013.502 Published online by Cambridge University Press

can be seen in appendix A that $\hat{f}_\eta, \hat{f}_\mu, \hat{f}_v, \hat{h}_v$ are odd and $\hat{f}_p, \hat{f}_d, \hat{h}_p, \hat{f}_u, \hat{h}_u$ are even. If

$$(\hat{\eta}_{j21})_{j=1} = -(\hat{\eta}_{j21})_{j=2}, \quad C_v = -D_v, \quad C_p = D_p, \tag{3.41}$$

then according to (3.24), (3.28), (3.29), (3.33) and (3.36), $\hat{v}_{21}$ will be odd and $\hat{u}_{21}$, $\hat{p}_{21}$, $\hat{p}_{gj21}$ even; this will make the boundary condition (3.37), (3.38) and (3.39) at $y = 1$ and $y = -1$ equivalent. Thus, both the number of equations and unknown constants reduce from 6 to 3. Solving them, one arrives at

$$\begin{aligned}\hat{\eta}_{j21} = -(-1)^j \Bigg\{ & \frac{(l_{21}^2 + 4k_1^2)\coth 2k_1}{2Rek_1(4k_1^2 - l_{21}^2)} \left[Re\left(\frac{\mathrm{d}\hat{h}_p}{\mathrm{d}y} + \hat{f}_v\right) - 2\mathrm{i}k_1\hat{f}_\mu + (4k_1^2 + l_{21}^2)\hat{f}_\eta \right] \\ & + \frac{4\mathrm{i}k_1 l_{21}\coth l_{21}}{Re\,(4k_1^2 - l_{21}^2)} \left[\frac{\mathrm{i}}{2k_1} Re\left(\frac{\mathrm{d}\hat{h}_p}{\mathrm{d}y} + \hat{f}_v\right) + \hat{f}_\mu + 4\mathrm{i}k_1\hat{f}_\eta - \frac{\mathrm{i}(4k_1^2 - l_{21}^2)}{2k_1}\hat{h}_v \right] \\ & + \hat{h}_p - \frac{2}{Re}\frac{\mathrm{d}\hat{h}_v}{\mathrm{d}y} + 2\rho\omega_1^2\hat{\eta}_{j1}^2 - \hat{f}_d \Bigg\}\Bigg|_{y=1} \frac{2k_1}{D_{var}(2\omega_1, 2k_1)}. \end{aligned} \tag{3.42}$$

The disturbances with $\exp(2\omega_{1i}t)$ in (3.21) can be solved in the same way, but as they do not contain the variable x, the process can be simplified. Proceeding with the same parity analysis, it is deduced that the disturbances with coefficient $\exp(2\omega_{1i}t)$ have the same parity as those with coefficient $\exp[2\mathrm{i}(k_1x - \omega_1 t)]$, so $\hat{v}_{22}$ is odd and $(\hat{\eta}_{j22})_{j=1} = -(\hat{\eta}_{j22})_{j=2}$. Substituting (3.21) into (2.23), collecting the terms with coefficient $\exp(2\omega_{1i}t)$ yields

$$\frac{\mathrm{d}\hat{v}_{22}}{\mathrm{d}y} = 0. \tag{3.43}$$

Noticing that $\hat{v}_{22}$ is odd, the solution of (3.43) gives

$$\hat{v}_{22} = 0. \tag{3.44}$$

Substituting (3.21) into (2.26), collecting the terms with coefficient $\exp(2\omega_{1i}t)$ yields

$$\hat{v}_{22} = 2\omega_{1i}\hat{\eta}_{j22} - \bar{\hat{\eta}}_{j1}\left(\mathrm{i}k_1\,\hat{u}_1 + \frac{\mathrm{d}\hat{v}_1}{\mathrm{d}y}\right) \quad \text{at } y = (-1)^{j+1}. \tag{3.45}$$

The bar on top of $\hat{\eta}_{j1}$ indicates the complex conjugate. Inserting (3.5) and (3.44) into (3.45) yields

$$\hat{\eta}_{j22} = 0. \tag{3.46}$$

The solutions of $\hat{u}_{22}$, $\hat{p}_{22}$, $\hat{\phi}_{gj22}$ and $\hat{p}_{gj22}$ can also be obtained using the same method; it is not necessary that they be zero. But focusing on the interface deformation, they are not noted. Hence, the interface disturbances generated from first-order disturbances have been derived.

Substituting the terms with coefficient $\exp[\mathrm{i}(2k_1 - \omega_2)t]$ in (3.21) into governing equations (2.23) to (2.31), it can be seen that they do not contain inhomogeneous nonlinear terms generated from the first order, so they are the same as equations in the first-order linear analysis, with k_1 and ω_1 replaced by $2k_1$ and ω_2. Similar properties apply to the terms with coefficient $\exp(-\mathrm{i}\omega_2' t)$. The non-trivial solution of

https://doi.org/10.1017/jfm.2013.502 Published online by Cambridge University Press

homogeneous equations is not single, so the initial condition is required. Substituting (2.12), (3.1) and (3.21) into initial condition (3.15) yields

$$\eta_0\hat{\eta}_{j1}\exp(\mathrm{i}k_1x)+\eta_0^2\left[(\hat{\eta}_{j21}+\hat{\eta}_{j23})\exp(2\mathrm{i}k_1x)+(\hat{\eta}_{j22}+\hat{\eta}_{j24})\right]=\tfrac{1}{2}\eta_0\exp(\mathrm{i}k_1x), \quad (3.47)$$

(3.47) yields

$$\hat{\eta}_{j1}=\tfrac{1}{2}, \quad \hat{\eta}_{j23}=-\hat{\eta}_{j21}, \quad \hat{\eta}_{j24}=-\hat{\eta}_{j22}=0, \quad (3.48)$$

and (3.48) indicates that $\hat{\eta}_{j22}$ and $\hat{\eta}_{j24}$ are zero, so according to (3.21), there are no purely time-dependent series in the second-order interface disturbance, and this is identical to the nonlinear solution for inviscid sheets presented by Clark & Dombrowski (1972) and Jazayeri & Li (2000). Because we have proved $(\hat{\eta}_{j21})_{j=1}=-(\hat{\eta}_{j21})_{j=2}$ in (3.41), according to (3.48), we have

$$\left(\hat{\eta}_{j23}\right)_{j=1}=-(\hat{\eta}_{j23})_{j=2}. \quad (3.49)$$

This means that the mode of second-order inherent instability is varicose. So, correspondingly, the dispersion relationship should be that of the varicose mode:

$$D_{var}(\omega_2, 2k_1)=0. \quad (3.50)$$

Hence ω_2 is obtained. Calculation results show that the second-order growth rate ω_{2i} is very small and negligible for two reasons. First, ω_{2i} is obtained from the varicose dispersion relation, so its value is inherently much smaller than the sinuous growth rate ω_{1i}. Second – and most importantly – it corresponds to the wavenumber $2k_1$. When k_1 acquires a relatively large number where the sheet is very unstable, $2k_1$ is always larger than the cut-off wavenumber, making ω_{2i} zero or negative. So in subsequent discussions, its property will not be noted. Clark & Dombrowski (1972) shared a similar opinion.

Finally, we have the expression for interface deformation:

$$\eta_j=\tfrac{1}{2}\eta_0\exp(\mathrm{i}k_1x-\mathrm{i}\omega_1t)+\eta_0^2(\hat{\eta}_{j21})_{\hat{\eta}_{j1}=1/2}\times\exp(2\mathrm{i}k_1x)[\exp(-2\mathrm{i}\omega_1t)-\exp(-\mathrm{i}\omega_2t)]+\mathrm{c.c.}, \quad (3.51)$$

where ω_1, $\hat{\eta}_{j21}$ and ω_2 are defined in (3.8), (3.42) and (3.50). The most important character of (3.51) is that according to (3.42) or (3.41), the second-order interface disturbance is varicose: this explains why the sinuous wave can disintegrate. According to the parity analysis, similar to the process of obtaining (3.41), it can be deduced that the third-order interface disturbance is also sinuous or antisymmetric, which is identical to the study presented by Jazayeri & Li (2000) for inviscid sheets. The third-order sinuous waves make the interface deformation more distorted but do not contribute to the thinning or breakup. So in terms of disintegration only, the third-order perturbation gives the same conclusion as the second-order perturbation, and the error of this analysis is fourth-order.

It can also be concluded that because the second-order growth rate ω_{2i} is very small and negligible, the first-order and second-order waves travel at the same velocity, explaining the phenomenon in which the thinning and the final breakup are at the same location of the fundamental wave.

The following is a comparison to the previous studies. The surface disturbances presented by Clark & Dombrowski (1972) and Jazayeri & Li (2000) can both be

https://doi.org/10.1017/jfm.2013.502 Published online by Cambridge University Press

expressed as

$$\eta_{j1} = \exp(\mathrm{i}k_1 x)[\hat{\eta}_{j11}\exp(-\mathrm{i}\omega_1 t) + \hat{\eta}_{j12}\exp(-\mathrm{i}\overline{\omega}_1 t)] + \text{c.c.}, \tag{3.52}$$

$$\eta_{j2} = \exp(2\mathrm{i}k_1 x)[\hat{\eta}_{j21}\exp(-2\mathrm{i}\omega_1 t) + \hat{\eta}_{j22}\exp(-2\mathrm{i}\overline{\omega}_1 t) + \hat{\eta}_{j23}\exp(-\mathrm{i}\omega_1 t - \mathrm{i}\overline{\omega}_1 t) + \hat{\eta}_{j24}\exp(-\mathrm{i}\omega_2 t) + \hat{\eta}_{j25}\exp(-\mathrm{i}\overline{\omega}_2 t)] + \text{c.c.} \tag{3.53}$$

Here

$$\omega_1 = -\alpha + \mathrm{i}\beta, \quad \overline{\omega}_1 = -\alpha - \mathrm{i}\beta, \tag{3.54}$$

where ω_1, $\overline{\omega}_1$ are two roots of dispersion relation (3.8) and ω_2, $\overline{\omega}_2$ are two roots of dispersion relation (3.50). The two roots of dispersion relation for inviscid sheets are complex conjugates when the temporal growth rate is positive. Setting ω_1 as the root with the positive growth rate, β is positive. Note that ω_1, ω_2, α, β, k_1 in (3.52), (3.53) and (3.54) correspond to non-dimensionalized $-n$, $-a$, α, β, k in the study of Clark & Dombrowski (1972), and $-\omega_1$, $-\omega_2$, α_1, β_1, k in the study of Jazayeri & Li (2000). As the normal mode exponent term in their study is '$\exp(\mathrm{i}kx + \mathrm{i}\omega t)$', the temporal frequencies ω_1, ω_2 in this paper are opposite in sign to those in their studies.

In (3.53), $\hat{\eta}_{j21}$, $\hat{\eta}_{j22}$, $\hat{\eta}_{j23}$ are the second-order disturbance amplitudes generated from the first-order disturbances and $\hat{\eta}_{j24}$, $\hat{\eta}_{j25}$ are the second-order inherent instability amplitudes. Similar to this paper, in (3.52) and (3.53), $\hat{\eta}_{j21}$, $\hat{\eta}_{j22}$, $\hat{\eta}_{j23}$ are obtained by solving inhomogeneous equations and $\hat{\eta}_{j11}$, $\hat{\eta}_{j12}$, $\hat{\eta}_{j24}$, $\hat{\eta}_{j25}$ are determined by initial conditions. Comparing (3.52) and (3.53) to (3.1) and (3.21), $\hat{\eta}_{j11}$ in (3.52) and $\hat{\eta}_{j21}$ and $\hat{\eta}_{j24}$ in (3.53) correspond to $\hat{\eta}_{j1}$ in (3.1) and $\hat{\eta}_{j21}$ and $\hat{\eta}_{j23}$ in (3.21). In this paper, we only consider the root of the dispersion relation (3.8) and (3.50) with a positive temporal growth rate (for (3.50), if the positive growth rate ω_{2i} exists); therefore (3.1) and (3.21) do not contain the terms corresponding to $\hat{\eta}_{j12}$, $\hat{\eta}_{j22}$, $\hat{\eta}_{j23}$ and $\hat{\eta}_{j25}$ in (3.52) and (3.53). Including the other root of the dispersion relation will make it possible to give another initial condition, i.e. the initial velocity condition. The different initial condition may also make $\hat{\eta}_{j24}$ in (3.53) different from $\hat{\eta}_{j23}$ in (3.21) in the present study. However, as the temporal growth rates of the disturbance component with amplitude $\hat{\eta}_{j12}$, $\hat{\eta}_{j22}$, $\hat{\eta}_{j23}$, $\hat{\eta}_{j24}$ and $\hat{\eta}_{j25}$ are either negative or too small, they do not contribute to instability. '$\hat{\eta}_{j21}\exp(2\mathrm{i}k_1 x - 2\mathrm{i}\omega_1 t)$' is the disturbance component that will cause the breakup of the sheet and it is only dependent on the first-order disturbance component '$\hat{\eta}_{j11}\exp(\mathrm{i}k_1 x - \mathrm{i}\omega_1 t)$'. Therefore, $\hat{\eta}_{j21}$ can be compared to the present study.

Clark & Dombrowski (1972) and Jazayeri & Li (2000) obtained $\hat{\eta}_{j11} = 1/4$ according to their chosen initial conditions. Setting $\hat{\eta}_{j1} = 1/4$, when viscosity vanishes, i.e. $Re \to \infty$, (3.42) reduces to

$$\hat{\eta}_{j21} = (-1)^{j+1}\frac{k_1\left\{(\omega_1 - k_1)^2\left[\frac{1}{2}\left(3 - \tanh^2 k_1\right) - 2\tanh k_1 \coth 2k_1\right] + \rho\omega_1^2\right\}}{8[D_{var}(2\omega_1, 2k_1)]_{Re\to\infty}}. \tag{3.55}$$

And when the second-order growth rate ω_{2i} is positive, according to the dispersion relation (3.14) and (3.50), (3.55) can be rewritten as

$$\hat{\eta}_{j21} = (-1)^{j}\frac{k_1\left\{(\omega_1 - k_1)^2\left[\frac{1}{2}\left(3 - \tanh^2 k_1\right) - 2\tanh k_1 \coth 2k_1\right] + \rho\omega_1^2\right\}}{8(\rho + \coth 2k_1)(-\omega_2 + 2\omega_1)(-\overline{\omega}_2 + 2\omega_1)}. \tag{3.56}$$

https://doi.org/10.1017/jfm.2013.502 Published online by Cambridge University Press

The result of Clark & Dombrowski (1972) is

$$\hat{\eta}_{j21} = (-1)^j \frac{P+Q}{4[-\omega_2 - 2(\alpha - \mathrm{i}\beta)][-\overline{\omega}_2 - 2(\alpha - \mathrm{i}\beta)]}, \tag{3.57}$$

where

$$P = \frac{\left[\beta^2 k_1 - (1+\alpha/k_1)^2 k^3\right]\left[\frac{1}{2}\left(3 - \tanh^2 k_1\right) - 2\tanh k_1 \coth 2k_1\right] + \rho k_1(\beta^2 - \alpha^2)}{2(\rho + \coth 2k_1)}, \tag{3.58a}$$

$$Q = \frac{2\mathrm{i}\beta k_1^2(1+\alpha/k_1)\left[\frac{1}{2}\left(3 - \tanh^2 k_1\right) - 2\tanh k_1 \coth 2k_1\right] + 2\mathrm{i}\alpha\beta\rho k_1}{2(\rho + \coth 2k_1)}. \tag{3.58b}$$

Note that $\hat{\eta}_{j21}$ in (3.57) corresponds to non-dimensionalized '$-((-1)^j A_7)/2$' in the study of Clark & Dombrowski (1972). Equation (3.57) has been non-dimensionalized from the original dimensional form. After simplification, (3.57) can be rewritten as

$$\hat{\eta}_{j21} = (-1)^{j+1} \frac{k_1\left\{(\omega_1 - k_1)^2\left[\frac{1}{2}\left(3 - \tanh^2 k_1\right) - 2\tanh k_1 \coth 2k_1\right] + \rho\omega_1^2\right\}}{8(\rho + \coth 2k_1)(-\omega_2 + 2\omega_1)(-\overline{\omega}_2 + 2\omega_1)}. \tag{3.59}$$

Comparing (3.56) to (3.59), we find that our result of $\hat{\eta}_{j21}$ is opposite in sign to that of Clark & Dombrowski (1972). We have also checked their inviscid analysis, but again obtained solutions identical to our study. This difference does not affect the breakup time, but as it causes a half-wavelength displacement of the second-order waves, the shape of the sheet deformation will not be the same.

The expression for $\hat{\eta}_{j21}$ presented by Jazayeri & Li (2000) is

$$\hat{\eta}_{j21} = (-1)^j \frac{\overline{C}}{(-\overline{\omega}_2 + 2\omega_1)(-\omega_2 + 2\omega_1)}, \tag{3.60}$$

$$C = -\frac{1}{32}\left(\tanh^2 k_1 + 4\coth 2k_1 \tanh k_1 - 5\right)\left(\overline{\omega}_1^2 - 2k_1\overline{\omega}_1 + k_1^2\right), \tag{3.61}$$

where $\hat{\eta}_{j21}$ in (3.60) corresponds to '$(-1)^j A_2$' in the study of Jazayeri & Li (2000). Equation (3.60) is different from both (3.56) and (3.59). This can be attributed to the difference in boundary conditions shown in appendix C. But we note that after careful examination, even using their boundary condition (C 9) in appendix C, the result we have derived is

$$\hat{\eta}_{j21} = (-1)^j \frac{2k_1\overline{C}}{(\rho + \coth 2k_1)(-\overline{\omega}_2 + 2\omega_1)(-\omega_2 + 2\omega_1)}, \tag{3.62}$$

$$C = -\frac{1}{32}\left(\tanh^2 k_1 + 4\coth 2k_1 \tanh k_1 - 5\right)\left(\overline{\omega}_1^2 - 2k_1\overline{\omega}_1 + k_1^2\right). \tag{3.63}$$

We conclude that the coefficient '$2k_1/(\rho + \coth 2k_1)$' was missed in their study, and '$k_1/(\rho + \coth 2k_1)$' exists in both (3.56) and (3.59).

3.3. *Second-order solutions for spatial instability*

In temporal instability analysis, the sheet considered is infinite and the disturbances grow with time at the same growth rate everywhere in space. But the most common

https://doi.org/10.1017/jfm.2013.502 Published online by Cambridge University Press

situation is a sheet emitted from a nozzle. In this case, the disturbances grow along the sheet. The spatial instability is more appropriate for describing this occurrence.

In spatial instability, the time frequency ω_1 is real and the wavenumber k_1 is complex. This means that at a fixed point, the sheet oscillates at the same amplitude and the disturbance amplitude grows with space at the growth rate $-k_{1i}$, which is the opposite number of k_1's imaginary part. This situation can be created by an external source of forcing on the sheet. Because Lin *et al.* (1990) showed that with ambient gas the sinuous mode of sheets is convectively unstable when the Weber number is larger than one, the disturbance that is impulsively introduced will finally die out at any fixed location; thus spatial instability can exist.

As the disturbance grows along the sheet, spatial instability is more approximate to the practical situation and can predict the disintegration length, which is of great practical use. Clark & Dombrowski (1972) noticed this and explained that spatial growing waves are more likely to be generated. But they did not discuss the spatial instability and they used Ut_d to estimate the breakup length, where U is the velocity of liquid sheets and t_d is the disintegration time in temporal instability. This method has been used by many other researchers as it is easy to understand and there were agreements with experiments, but the physical meaning is not very clear and it does not give any information on the deformation of the sheets. Jazayeri & Li (2000) and Ibrahim & Jog (2008) transformed the solution for temporal instability into the solution for spatial instability according to the relation between temporal and spatial growth rate presented by Gaster (1962). However, this method may not be adequate for nonlinear analysis because based on the solution for linear analysis, Gaster's (1962) transformation does not give any information about the nonlinear terms. Furthermore, Gaster (1962) himself noted: 'these relations do not constitute a transformation of a time-dependent solution into a spatially-dependent one, but merely provide a link between the values of the parameters existing in two problems'. The 'parameters existing in two problems' refer to the temporal and spatial growth rate. Therefore, we shall give an exact second-order solution for spatial instability.

The initial condition (3.15) for temporal instability may not fit the spatial instability, as the interface deformation does not evolve with time. Instead, a boundary condition should be introduced to indicate the external forcing:

$$(\eta_j)_{j=1}|_{x=0} = (\eta_j)_{j=2}|_{x=0} = \eta_0 \cos \omega_1 t = \tfrac{1}{2}\eta_0 \exp(-\mathrm{i}\omega_1 t) + \text{c.c.} \tag{3.64}$$

The sinuous mode is still chosen according to linear analysis. The first-order solutions are the same as those in temporal analysis, but the wavenumber k_1 is now complex and the temporal frequency ω_1 is real. So, similar to (3.16)–(3.20), the nonlinear terms generated from the first-order solutions are expressed as

$$\hat{f}' \exp[2\mathrm{i}(k_1 x - \omega_1 t)] + \hat{g}' \exp(-2k_{1i}x) + \text{c.c.} \tag{3.65}$$

Therefore, considering the boundary condition (3.64), the second-order interface disturbance is assumed to be

$$\begin{aligned}\eta_{j2} = {} & \hat{\eta}'_{j21} \exp[2\mathrm{i}(k_1 x - \omega_1 t)] + \hat{\eta}'_{j22} \exp(-2k_{1i}x) \\ & + \hat{\eta}'_{j23} \exp[\mathrm{i}(k_2 x - 2\omega_1 t)] + \hat{\eta}'_{j24} \exp(\mathrm{i}k'_2 x) + \text{c.c.},\end{aligned} \tag{3.66}$$

where k_2 and k'_2 are the second-order wavenumbers. $\hat{\eta}'_{j21}$ and $\hat{\eta}'_{j22}$ are solved using the same method as temporal instability and they are given in appendix B. Substituting (2.12), (3.1) and (3.66) into boundary condition (3.64), $\hat{\eta}'_{j1}$, $\hat{\eta}'_{j23}$ and $\hat{\eta}'_{j24}$ can be solved

https://doi.org/10.1017/jfm.2013.502 Published online by Cambridge University Press

to give

$$\hat{\eta}_{j1} = \tfrac{1}{2}, \quad \hat{\eta}'_{j23} = -\hat{\eta}'_{j21}, \quad \hat{\eta}'_{j24} = -\hat{\eta}'_{j22}. \tag{3.67}$$

According to (3.67), the second-order interface disturbance for spatial instability is also varicose, so the second-order complex wavenumber is solved according to the dispersion relation

$$D_{var}(2\omega_1, k_2) = 0 \quad \text{and} \quad D_{var}\left(0, k'_2\right) = 0 \tag{3.68}$$

where $D_{var}(0, k'_2) = 0$ yields

$$k'_2 = 0. \tag{3.69}$$

So the interface disturbance for spatial instability is

$$\eta_j = \tfrac{1}{2}\eta_0 \exp(\mathrm{i}k_1 x - \mathrm{i}\omega_1 t) + \eta_0^2\left(\hat{\eta}'_{j21}\right)_{\hat{\eta}_{j1}=1/2} \exp(-2\mathrm{i}\omega_1 t)[\exp(2\mathrm{i}k_1 x) - \exp(\mathrm{i}k_2 x)]$$
$$+ \eta_0^2\left(\hat{\eta}'_{j22}\right)_{\hat{\eta}_{j1}=1/2}[\exp(-2k_{1i}x) - 1] + \text{c.c.} \tag{3.70}$$

Comparing (3.70) to (3.51), it can be seen that the solution for spatial instability does not have a second-order temporal frequency ω_2 but has a second-order wavenumber k_2 instead. The second-order spatial growth rate $-k_{2i}$ is also very small and negligible. Calculation results show that at the same real wavenumber, the second-order interface disturbance amplitudes of spatial and temporal instability are nearly the same:

$$\hat{\eta}'_{j21}(k_{1r} + \mathrm{i}k_{1i}) \approx \hat{\eta}_{j21}(k_{1r}), \quad \hat{\eta}'_{j22}(k_{1r} + \mathrm{i}k_{1i}) \approx \hat{\eta}_{j22}(k_{1r}) = 0. \tag{3.71}$$

This may be because the spatial or temporal growth rate is very small compared to the frequency of oscillation, i.e. $|k_{1i}| \ll |k_{1r}|$, and this makes

$$k_{1r} + \mathrm{i}k_{1i} \approx k_{1r}. \tag{3.72}$$

As the second-order disturbance amplitude is a function of complex wavenumber k_1, (3.71) can be derived according to (3.72). This explains the phenomenon that interface deformation for temporal and spatial instability is nearly the same at the same wavelength. As the conclusions from temporal and spatial instability are very similar, they will be discussed together.

4. Results and discussion

Using the second-order solution, more features of sinuous wave growth can be obtained. Figure 2 shows the temporal evolution of sinuous interface waves of a viscous sheet at a Weber number of 400, a Reynolds number of 1000, a gas-to-liquid density ratio of 0.001 and initial disturbance of 0.1. The wavenumber is chosen to be 0.23, which is equal to the dominant wavenumber for the sinuous disturbance according to linear analysis. It can be seen that the wave amplitude grows and maintains the sinuous character for the majority of the time. The distance between the two interfaces remains almost a constant until the dimensionless time of 400. Then the nonlinear effect becomes significant and the wave becomes more distorted. At a time of 500, distinct thinnings appear on the sheet. Finally at 547, the two interfaces touch each other and the sheet breaks up, resulting in ligaments interspaced by half a wavelength.

We focus on the parameters in the second-order interface disturbances because the second-order surface deformation is varicose (or dilatational) and this is the cause of the disintegration. Because the conclusions of temporal and spatial instability are very

https://doi.org/10.1017/jfm.2013.502 Published online by Cambridge University Press

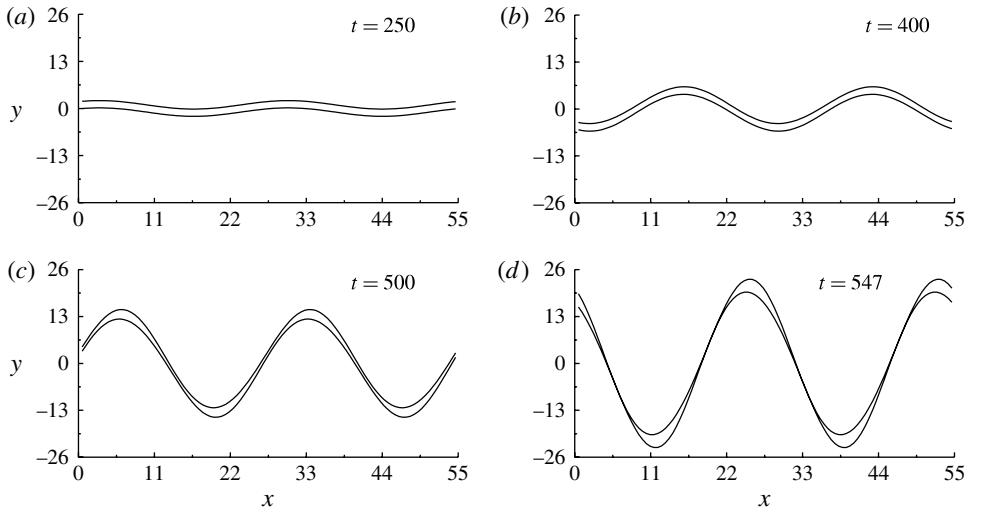


FIGURE 2. Temporal evolution of sinuous waves at $k_1 = 0.23$, $We = 400$, $Re = 1000$, $\rho = 0.001$, $\eta_0 = 0.1$: (*a*) $t = 250$, (*b*) $t = 400$, (*c*) $t = 500$, (*d*) $t = 547$.

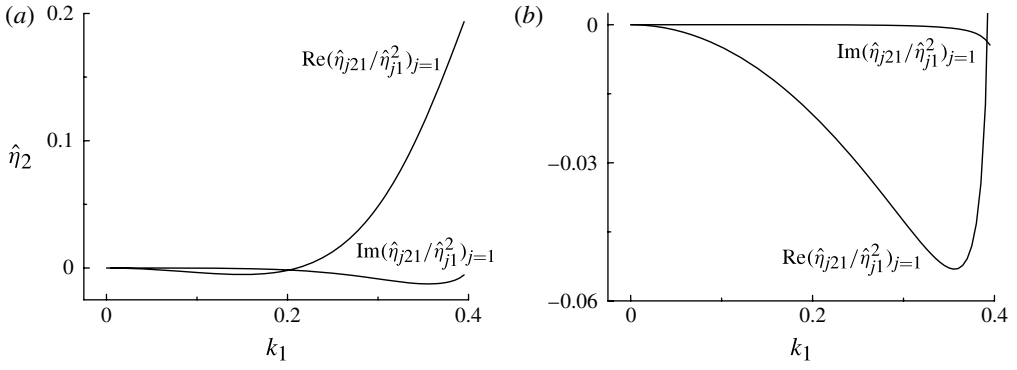


FIGURE 3. Real and imaginary part of $\hat{\eta}_{j21}/\hat{\eta}_{j1}^2$ at $We = 400$, $\rho = 0.001$: (*a*) $Re \to \infty$, (*b*) $Re = 1$.

similar, only the parameters in temporal instability will be investigated. According to (3.51), as we have proved that ω_{2i} is negligible, the first-order complex temporal frequency ω_1 and the second-order initial amplitude $\hat{\eta}_{j21}$ are the key factors affecting the second-order interface disturbances. While ω_{1i} represents the temporal exponential growth rate, $\hat{\eta}_{j21}$ indicates the nonlinear effects. The initial disturbance η_0 is assumed to be 0.1, according to the experiment conducted by Clark & Dombrowski (1972), in which the initial disturbance is of the order of 10^{-4} m, and the widths of most nozzles are of the order of 1 mm. The value of the initial disturbance will affect the breakup time or length, but does not change the breakup character or the effect of Weber number, Reynolds number or gas-to-liquid density ratio.

Here $\hat{\eta}_{j21}$ is in proportion to the square of $\hat{\eta}_{j1}$, so $\hat{\eta}_{j21}/\hat{\eta}_{j1}^2$ will be used to judge the ratio of the first harmonic to the fundamental disturbances; $\hat{\eta}_{j21}/\hat{\eta}_{j1}^2$ is a complex number, its real and imaginary parts for two typical conditions are shown in figure 3. The absolute value of the real part of $\left(\hat{\eta}_{j21}/\hat{\eta}_{j1}^2\right)_{j=1}$ is much larger than its imaginary

https://doi.org/10.1017/jfm.2013.502 Published online by Cambridge University Press

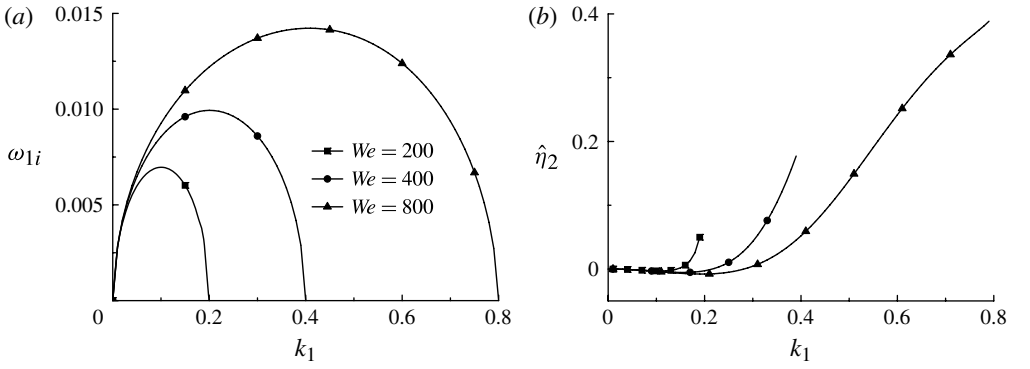


FIGURE 4. The effect of Weber number on (a) dispersion relation and (b) initial amplitude of second-order interface disturbance at $Re = 1000$, $\rho = 0.001$.

part, and this also holds for other situations. Therefore, we set

$$\hat{\eta}_2 = \mathrm{Re}\left(\frac{\hat{\eta}_{j21}}{\hat{\eta}_{j1}^2}\right)_{j=1} \tag{4.1}$$

and $\hat{\eta}_2$ will be used to represent the second-order initial disturbance amplitude in the following study.

Figure 4(a) shows the dispersion relation (temporal instability) at different Weber numbers. It can be seen that a larger Weber number increases the temporal growth rate drastically and results in a broader range of unstable wavenumbers as well. The dominant wavenumber, which is the wavenumber corresponding to the maximum growth rate, also increases with the Weber number. As instability is mainly caused by amplification of the disturbance amplitude, the focus here is on the situation in which the temporal and spatial growth rates are positive. The capillary wave distortion in which the disturbance amplitude remains the same, studied by Mehring & Sirignano (1999), will not be discussed here.

Figure 4(b) shows the second-order initial amplitude $\hat{\eta}_2$ as a function of wavenumber k_1 (temporal instability); $|\hat{\eta}_2|$ generally increases with k_1, indicating that shorter waves have stronger nonlinear effects. The wavenumber range is chosen to be the range of the unstable wave with positive temporal growth rate according to figure 4(a). A larger Weber number provides a broader unstable wavenumber range, so $|\hat{\eta}_2|$ can acquire a much larger value. Hence the Weber number will contribute greatly to both the temporal growth rate and the second-order initial disturbance amplitude, greatly enhancing the instability.

The breakup time t_d as a function of wavenumber k_1 is shown in figure 5. With the increase of wavenumber, the breakup time first decreases and then increases towards infinity, when the wavenumber approaches the cut-off wavenumber. This is because the disturbance is amplified only when the temporal growth rate ω_{1i} is positive. Obviously, a larger Weber number results in a much shorter breakup time and greatly enhances instability.

Figure 6 is a comparison of the most unstable wavelength predicted by linear and nonlinear analysis. The Ohnesorge number, $Z = \mu/\sqrt{\rho_l a \sigma}$, is chosen according to the property of water at $a = 1$ mm; thus different Weber numbers represent different velocities. According to linear analysis, the most unstable wave is that which has the

https://doi.org/10.1017/jfm.2013.502 Published online by Cambridge University Press

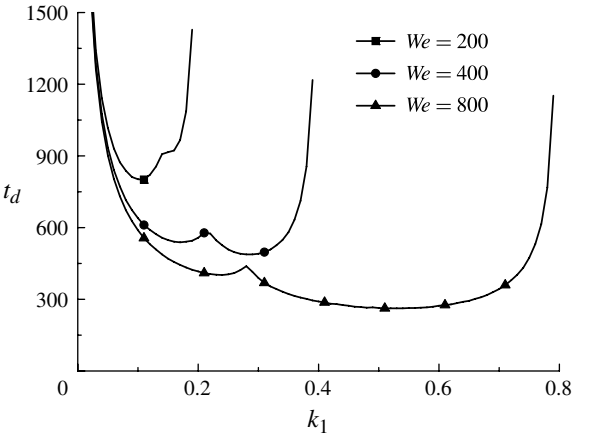


FIGURE 5. The effect of Weber number on breakup time at $Re = 1000$, $\rho = 0.001$.

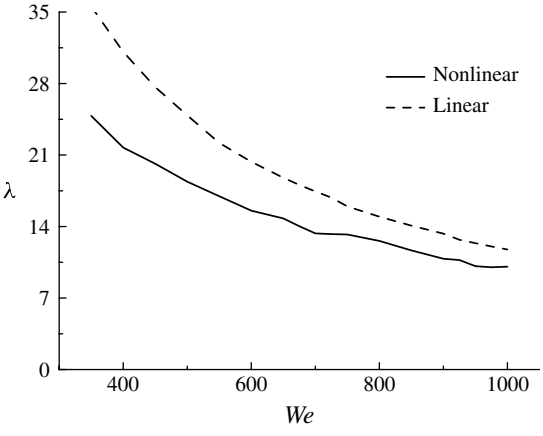


FIGURE 6. Comparison of the most unstable wavelength predicted by linear and nonlinear analysis at $Z = 0.0037$, $\rho = 0.001$.

largest temporal growth rate ω_{1i}. This idea was first suggested by Rayleigh (1879) in the linear stability analysis of cylinder jets. For the weakly nonlinear analysis in this paper, the wave with the shortest breakup time t_d is the most unstable. It can be seen that the most unstable wave predicted by nonlinear analysis is slightly shorter under the chosen conditions. This is because according to figure 4(*b*), a shorter wave has a larger second-order initial amplitude $|\hat{\eta}_2|$. This may provide an explanation for the phenomenon observed by Heislbetz, Madlener & Ciezki (2007) and Yang *et al.* (2012) that the measured wavelength is smaller than the theoretical dominant wavelength predicted by linear analysis when the Weber number is not very large.

The interface deformation at breakup time (temporal instability) at different Weber numbers is shown in figure 7. The wavenumber k_1 is chosen to be that with the shortest breakup time t_d. With the increase of Weber number, the breakup time reduces significantly and the interface deformation becomes more distorted, gradually changing from a nearly sinuous wave into a sawtooth-like shape. This is due to the increase of

https://doi.org/10.1017/jfm.2013.502 Published online by Cambridge University Press

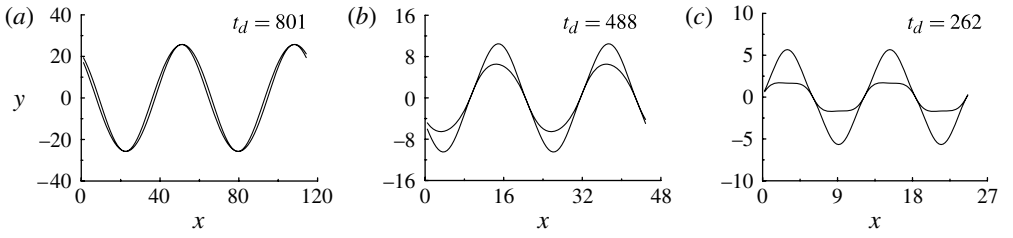


FIGURE 7. The shape of interface deformation at breakup time for different Weber numbers, $Re = 1000$, $\rho = 0.001$: (*a*) $We = 200$, $k_1 = 0.11$, $t_d = 801$; (*b*) $We = 400$, $k_1 = 0.28$, $t_d = 488$; (*c*) $We = 800$, $k_1 = 0.51$, $t_d = 262$.

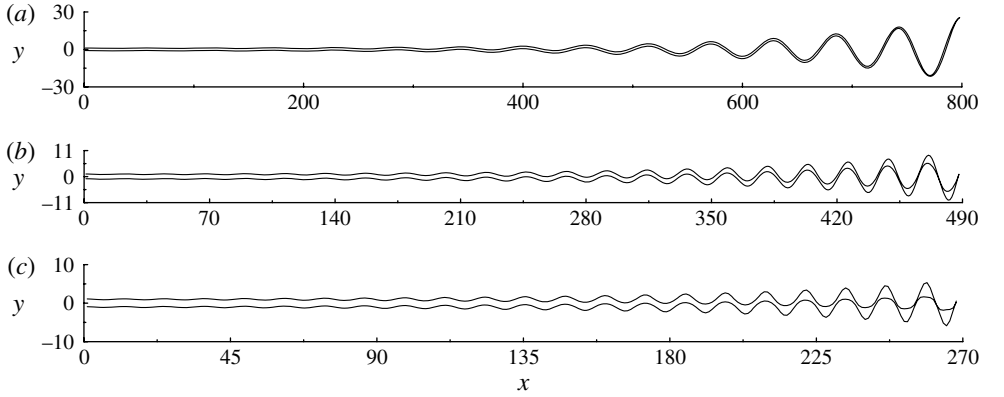


FIGURE 8. Spatial evolution of interface deformation for different Weber numbers at $Re = 1000$, $\rho = 0.001$: (*a*) $We = 200$, $k_1 = 0.11 - 0.0069\mathrm{i}$, $l_d = 798$; (*b*) $We = 400$, $k_1 = 0.28 - 0.0091\mathrm{i}$, $l_d = 488$; (*c*) $We = 800$, $k_1 = 0.51 - 0.014\mathrm{i}$, $l_d = 268$.

$|\hat{\eta}_2|$, making the nonlinear effect more prominent. The spatial instability of the same parameters and wavelengths is shown in figure 8. The evolution of the disturbance is clearly observed until the location of disintegration. The breakup length is defined as l_d. Similar to temporal instability, a larger Weber number results in a significantly smaller breakup length and a more distorted interface deformation. It can be seen that the non-dimensional breakup length nearly coincides with the non-dimensional breakup time in temporal instability, and the shape of the wave near the breakup region is also very similar to that of temporal instability. Therefore the temporal and spatial instability give the same conclusion.

Figure 9 is a comparison of figure 8(*b*) at a different wavelength. The Weber number, Reynolds number and gas-to-liquid density ratio in figure 9 are the same as those in figure 8(*b*), but the wave in figure 9 is longer. According to dispersion relation (3.8), a different wavenumber k_1 can be created by giving a different oscillating frequency ω_1 in the boundary condition (3.64) for spatial instability. Compared to figure 8(*b*), the wave in figure 9 is less distorted because according to figure 4(*b*), a longer wave has a smaller nonlinear amplitude $|\hat{\eta}_2|$. Although the wave in figure 9 has the largest spatial growth rate and is therefore the most unstable according to linear analysis, the breakup length is longer than that of figure 8(*b*). This also proves that the most unstable wave predicted by nonlinear analysis is different from linear analysis.

https://doi.org/10.1017/jfm.2013.502 Published online by Cambridge University Press

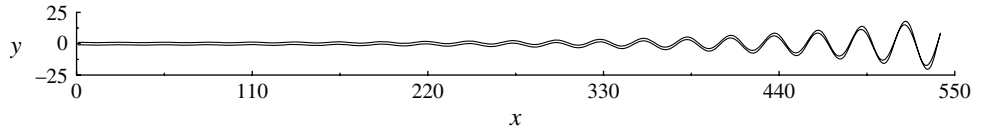


FIGURE 9. Spatial evolution of interface deformation at $We = 400$, $k_1 = 0.23 - 0.0098\mathrm{i}$, $Re = 1000$, $\rho = 0.001$, $l_d = 541$.

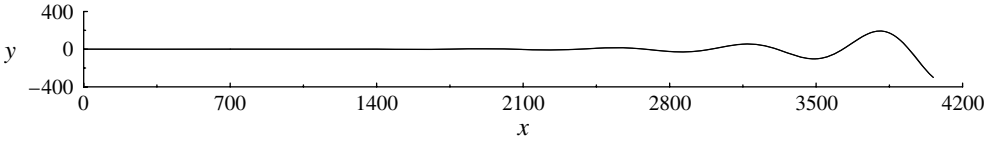


FIGURE 10. Spatial evolution of interface deformation at $We = 20$, $k_1 = 0.010 - 0.0020\mathrm{i}$, $Re = 1000$, $\rho = 0.001$, $l_d = 4060$.

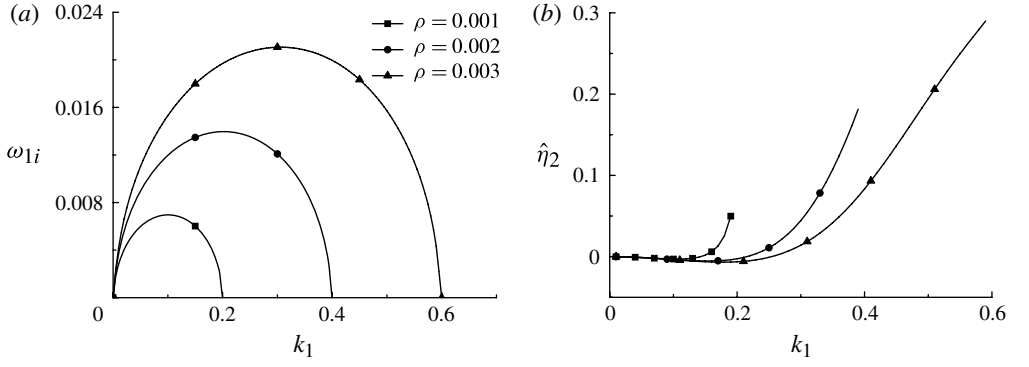


FIGURE 11. The effect of gas-to-liquid density ratio on (*a*) dispersion relation and (*b*) initial amplitude of second-order interface disturbance at $Re = 1000$, $We = 200$.

When the Weber number becomes very small, e.g. smaller than 50, both ω_{1i}, or $-k_{1i}$ and $|\hat{\eta}_2|$ are so small that it takes a very long time, or distance, to disintegrate: see figure 10. If the width of the nozzle (the dimension scale of length) is not very small, e.g. around 1 mm, the breakup length will be several metres. Therefore the instability may not be easily observed as the wavelength is too long and the amplitude is so small in practical finite space. This can explain the experimental conclusion presented by Mouis (2003), that the sheets in the stationary gas medium with Weber numbers smaller than 50 are in the smooth regime, where the sheet is stable and few wave motions can be observed, although theoretically the sheet is convectively unstable at Weber numbers larger than one (Lin *et al.* 1990). But if the width of the nozzle is very small, e.g. of the order of 10^{-4} cm (like the experiment conducted by Squire 1953), the length dimension scale is greatly reduced and the wave instability is still visible and distinct.

The effect of the gas-to-liquid density ratio is shown in figures 11–14. A larger gas density enlarges the temporal growth rate ω_{1i} and the second-order initial disturbance

https://doi.org/10.1017/jfm.2013.502 Published online by Cambridge University Press

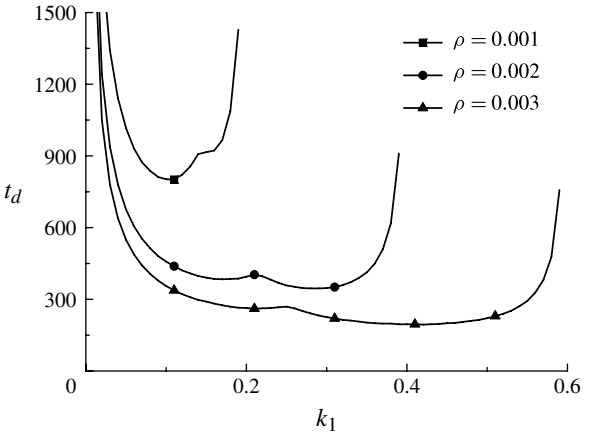


FIGURE 12. The effect of gas-to-liquid density ratio on breakup time at $Re = 1000$, $We = 200$.

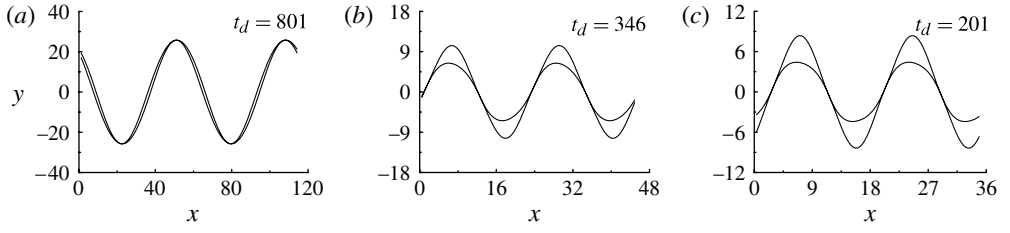


FIGURE 13. The shape of interface deformation at breakup time for different gas-to-liquid density ratios, $Re = 1000$, $We = 200$: (*a*) $\rho = 0.001$, $k_1 = 0.11$, $t_d = 801$; (*b*) $\rho = 0.002$, $k_1 = 0.28$, $t_d = 346$; (*c*) $\rho = 0.003$, $k_1 = 0.36$, $t_d = 201$.

amplitude $|\hat{\eta}_2|$, resulting in a much shorter disintegration time or length, and a more distorted interface deformation. So the effect of gas-to-liquid density ratio is very similar to the effect of Weber number. Under the chosen conditions, the destabilizing effect of the gas-to-liquid density ratio is even stronger than that of Weber number.

Figure 15 shows the spatial evolution of interface deformation at a very small gas-to-liquid density ratio $\rho = 10^{-4}$. Similar to the case of small Weber number, the sheet takes a very long distance to disintegrate so that it seems nearly stable in common finite space. Again, this is identical to the experiment conducted by Squire (1953), in that the breakup is not caused by wave motion at small gas-to-liquid density ratios, although theoretically the sheet is convectively unstable when $We > 1$ as long as the ambient gas exists (Lin *et al.* 1990). The present study only focuses on wave disintegration, whereas there are two other forms of disintegration, i.e. rim and perforated-sheet disintegration (Fraser & Eisenklam 1953). Previous studies (Sirignano & Mehring 2000) have shown that the wave disintegration is caused by aerodynamic interaction with the surrounding gas. This is identical to the present study in which wave instability is distinct only at relatively large Weber numbers and gas-to-liquid density ratios. The rupture of liquid sheets or films studied by Prévost & Gallez (1986), Erneux & Davis (1993), De Wit *et al.* (1994), Sharma *et al.* (1995), Hwang *et al.* (1996), Lin *et al.* (2000), Vaynblat *et al.* (2001), Yoshinaga & Uchiyama (2001)

https://doi.org/10.1017/jfm.2013.502 Published online by Cambridge University Press

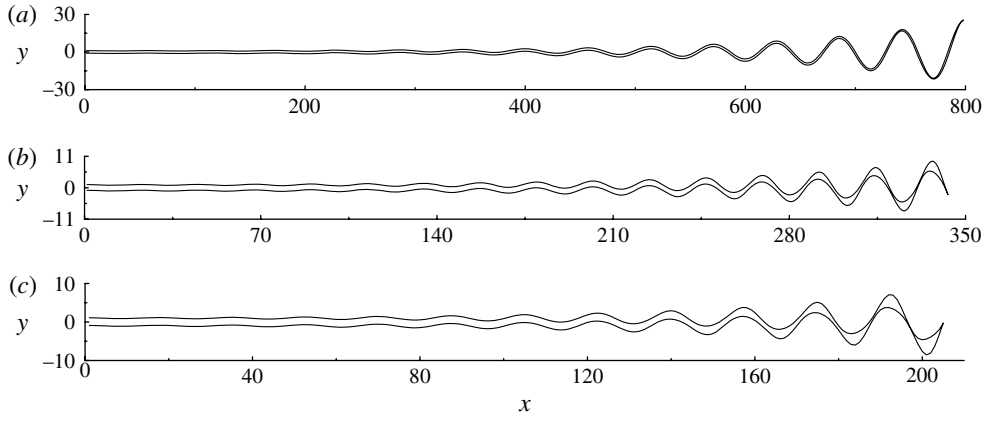


FIGURE 14. Spatial evolution of interface deformation for different gas-to-liquid density ratios at $Re = 1000$, $We = 200$: (*a*) $\rho = 0.001$, $k_1 = 0.11 - 0.0069\mathrm{i}$, $l_d = 798$; (*b*) $\rho = 0.002$, $k_1 = 0.28 - 0.013\mathrm{i}$, $l_d = 343$; (*c*) $\rho = 0.003$, $k_1 = 0.36 - 0.021\mathrm{i}$, $l_d = 205$.

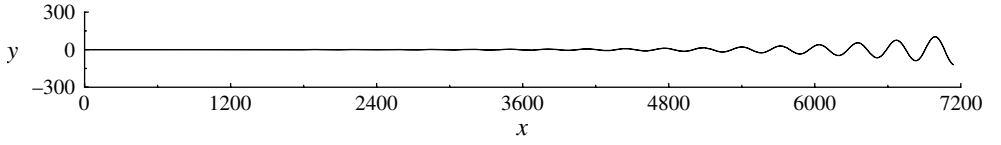


FIGURE 15. Spatial evolution of interface deformation at $\rho = 10^{-4}$, $We = 400$, $Re = 1000$, $k_1 = 0.020 - 0.0010\mathrm{i}$, $l_d = 7140$.

and Yoshinaga & Yoshida (2003) can also be attributed to wave disintegration, but these wave instabilities are not caused by the ambient gas, as the ambient gas has been neglected in their analyses. They are caused by other factors such as van der Waals forces or temperature differences.

The effect of Reynolds number is examined next. In the experiment of Hagerty & Shea (1955) and Tammisola *et al.* (2011), the Weber number was approximately 300 and 500 respectively, while the gas-to-liquid density ratio was the ratio of air to water. Their linear stability analyses agreed well with their experiments. Therefore, $We = 400$ and $\rho = 0.001$ is chosen as a typical condition to study the effect of Reynolds number. The Weber number remains a constant for different Reynolds numbers, so the effect of Reynolds number represents the effect of viscosity.

The dispersion relations for different Reynolds numbers are shown in figure 16(*a*). The temporal growth rate decreases with the decreased Reynolds number, so the linear theory concludes that viscosity has a stabilizing effect. Figure 16(*a*) also indicates that the stabilizing effect of viscosity is very weak at large Reynolds numbers, but becomes stronger at small Reynolds numbers.

The second-order disturbance amplitude $\hat{\eta}_2$ at different Reynolds numbers is shown in figure 16(*b*). Here $|\hat{\eta}_2|$ first decreases as the Reynolds number decreases from infinity to $\sim$150. However, in the most unstable wavenumber range (the range with the shortest breakup time, approximately $0.1 < k_1 < 0.3$), a further reduction of Reynolds number makes $\hat{\eta}_2$ negative and the absolute value of $\hat{\eta}_2$, $|\hat{\eta}_2|$ again increases. Hence viscosity reduces nonlinear disturbance amplitudes at large Reynolds numbers but

https://doi.org/10.1017/jfm.2013.502 Published online by Cambridge University Press

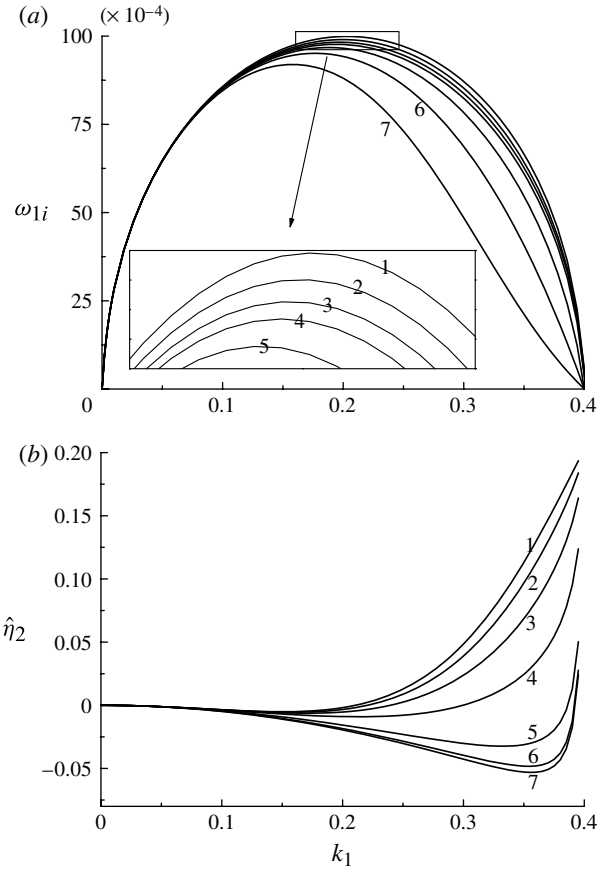


FIGURE 16. The effect of Reynolds number on (*a*) dispersion relation and (*b*) initial amplitude of second-order interface disturbance at $We = 400$, $\rho = 0.001$: curve 1, $Re = \infty$; curve 2, $Re = 500$; curve 3, $Re = 150$; curve 4, $Re = 50$; curve 5, $Re = 10$; curve 6, $Re = 3$; curve 7, $Re = 1$.

enhances nonlinear amplitudes at smaller Reynolds numbers. Figure 16(*b*) also shows that the variation of $\hat{\eta}_2$ at different Reynolds numbers is prominent when the Reynolds number is between approximately 10 and 150; $\hat{\eta}_2$ is insensitive to Reynolds number when the Reynolds number is very large or very small.

The overall effect of Reynolds number is assessed by the breakup time (for temporal instability), shown in figure 17. The effect of Reynolds number varies among different ranges of Reynolds numbers. When the Reynolds number is larger than 150, viscosity reduces both the temporal growth rate ω_{1i} and the second-order disturbance amplitude $|\hat{\eta}_2|$. Therefore, as shown in figure 17(*a*), a decrease of Reynolds number leads to an increase of breakup time. When the Reynolds number becomes smaller than $\sim$150, the effects of viscosity on the temporal growth rate and the second-order amplitude become opposite: according to the discussion above, viscosity reduces temporal growth rate but enhances the second-order amplitude. Figure 17(*b*) indicates that when the Reynolds number is between 10 and 150, a reduction of Reynolds number leads to a decrease of breakup time. This can be explained by figure 16: the destabilizing effect of viscosity on $|\hat{\eta}_2|$ is pronounced but the stabilizing effect of viscosity on ω_{1i} is

https://doi.org/10.1017/jfm.2013.502 Published online by Cambridge University Press

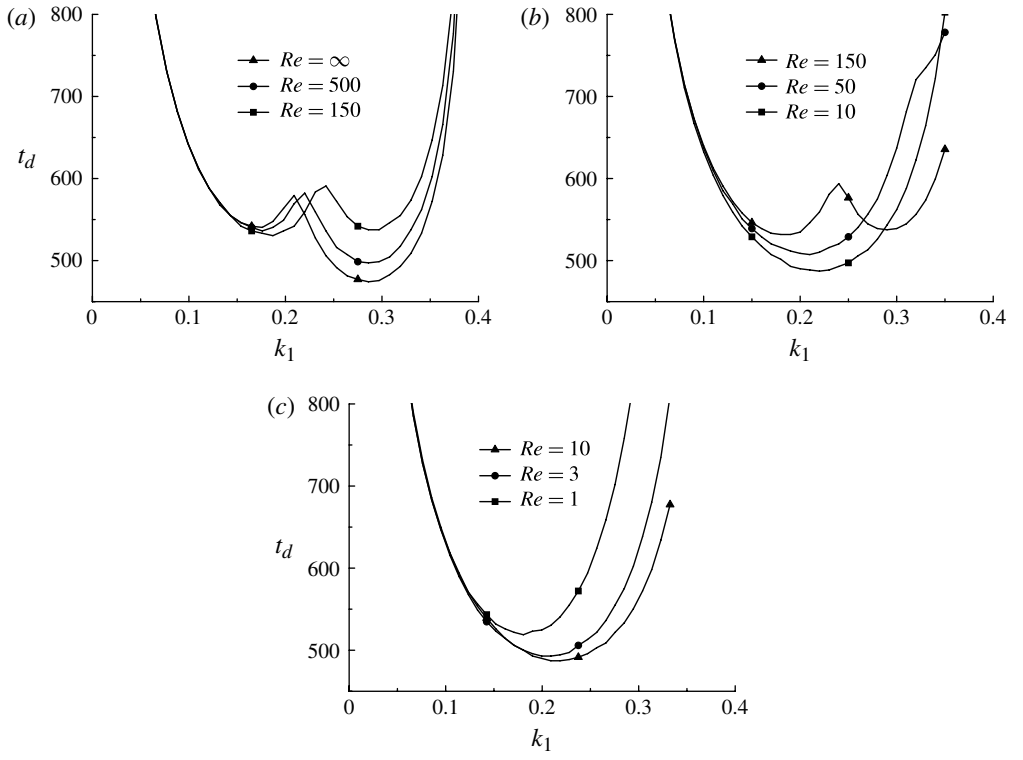


FIGURE 17. The effect of Reynolds number on breakup time at $We = 400$, $\rho = 0.001$: (*a*) $Re \geqslant 150$, (*b*) $10 \leqslant Re \leqslant 150$, (*c*) $Re \leqslant 10$.

relatively minor when $10 \leqslant Re \leqslant 150$. Figure 17(*c*) displays that when the Reynolds number is smaller than 10, a reduction of Reynolds number leads to an increase of breakup time. This can also be attributed to the trend shown in figure 16: when the Reynolds number is very small, the stabilizing effect of viscosity on ω_{1i} becomes prominent and dominates over the effect of $\hat{\eta}_2$. In summary, under the condition of $We = 400$ and $\rho = 0.001$, viscosity has a stabilizing effect when the Reynolds number is approximately larger than 150 or smaller than 10. When the Reynolds number is between 150 and 10, viscosity has a destabilizing effect.

Figures 18 and 19 show the deformations at different Reynolds numbers. The wavelength is the one with the shortest breakup time for temporal instability. The variation of breakup length with different Reynolds numbers shown in figure 19 is generally identical to the breakup time discussed in figure 17. For $Re \geqslant 500$, $\hat{\eta}_2$ is positive at the chosen wavenumber; therefore according to (3.51), (3.70) and (4.1), the sheet breaks up at the positions corresponding to a half and full wavelength of the fundamental sinuous wave. For $Re \leqslant 150$, $\hat{\eta}_2$ is negative at the chosen wavenumber, so the sheet breaks up at the positions corresponding to $1/4$ and $3/4$ of the wavelength of the fundamental sinuous wave.

For other Weber numbers or gas-to-liquid density ratios, the effect of Reynolds number or viscosity is similar to figure 17, although it is not necessary that the critical Reynolds numbers be 150 and 10. But note that for small Weber numbers and gas-to-liquid density ratios, i.e. when $\rho We < 0.2$, $\hat{\eta}_2$ is already negative for inviscid

https://doi.org/10.1017/jfm.2013.502 Published online by Cambridge University Press

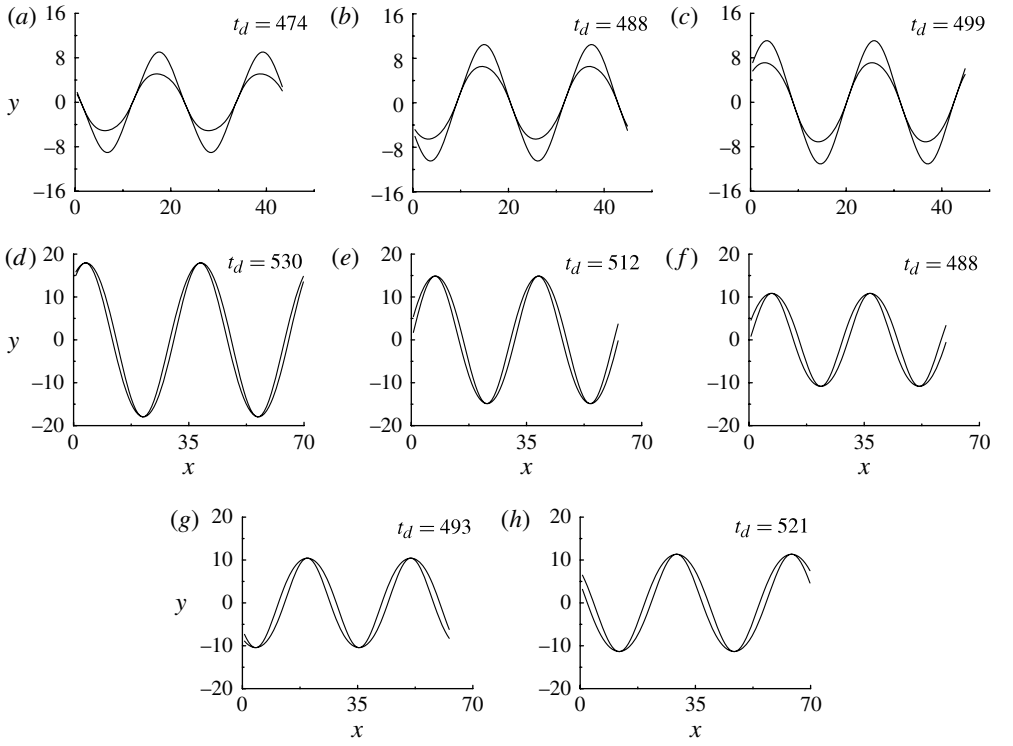


FIGURE 18. The shape of interface deformation at breakup time for different Reynolds numbers at $We = 400$, $\rho = 0.001$: (*a*) $Re = \infty$, $k = 0.29$, $t_d = 474$; (*b*) $Re = 1000$, $k = 0.28$, $t_d = 488$; (*c*) $Re = 500$, $k = 0.28$, $t_d = 499$; (*d*) $Re = 150$, $k = 0.18$, $t_d = 530$; (*e*) $Re = 50$, $k = 0.20$, $t_d = 512$; (*f*) $Re = 10$, $k = 0.21$, $t_d = 488$; (*g*) $Re = 3$, $k = 0.20$, $t_d = 493$; (*h*) $Re = 1$, $k = 0.18$, $t_d = 521$.

liquid in most wavenumbers (see figure 20); viscosity only enhances the nonlinear amplitude. Therefore, the regime shown in figure 17(*a*), in which the viscosity plays a stabilizing role at large Reynolds numbers, vanishes under this condition. Viscosity plays a weak destabilizing role at large Reynolds numbers and a weak stabilizing role at small Reynolds numbers. Also note that, in fact, the breakup time and wave deformation vary only a little for different Reynolds numbers under this condition (see figure 21); the effect of viscosity is too weak and virtually negligible.

The effect of viscosity is somewhat complicated and different from the normal expectation that viscosity only tends to damp out or dissipate disturbances. But there have already been studies showing the destabilizing effect of viscosity. For viscous sheets, the linear instability analysis of Lin (1981), Li & Tankin (1991) and Li (1993) have all concluded that the viscosity plays a dual role on the sheet instability. Li & Tankin (1991) also listed three other situations in which the fluid viscosity may have a destabilizing effect depending on the flow conditions: planar Poiseuille flow, studied by Heisenberg (1924), Blasius flow studied by Schlichting (1933) and Tollmien (1929), and the Bénard problem (thermal instability of a layer of fluid heated from below) under constant rotation studied by Chandrasekhar (1961). Drazin (2002) made a detailed study of the effect of viscosity on the stability of parallel flows and the Orr–Sommerfeld problem. It has been clearly shown that viscosity may render

https://doi.org/10.1017/jfm.2013.502 Published online by Cambridge University Press

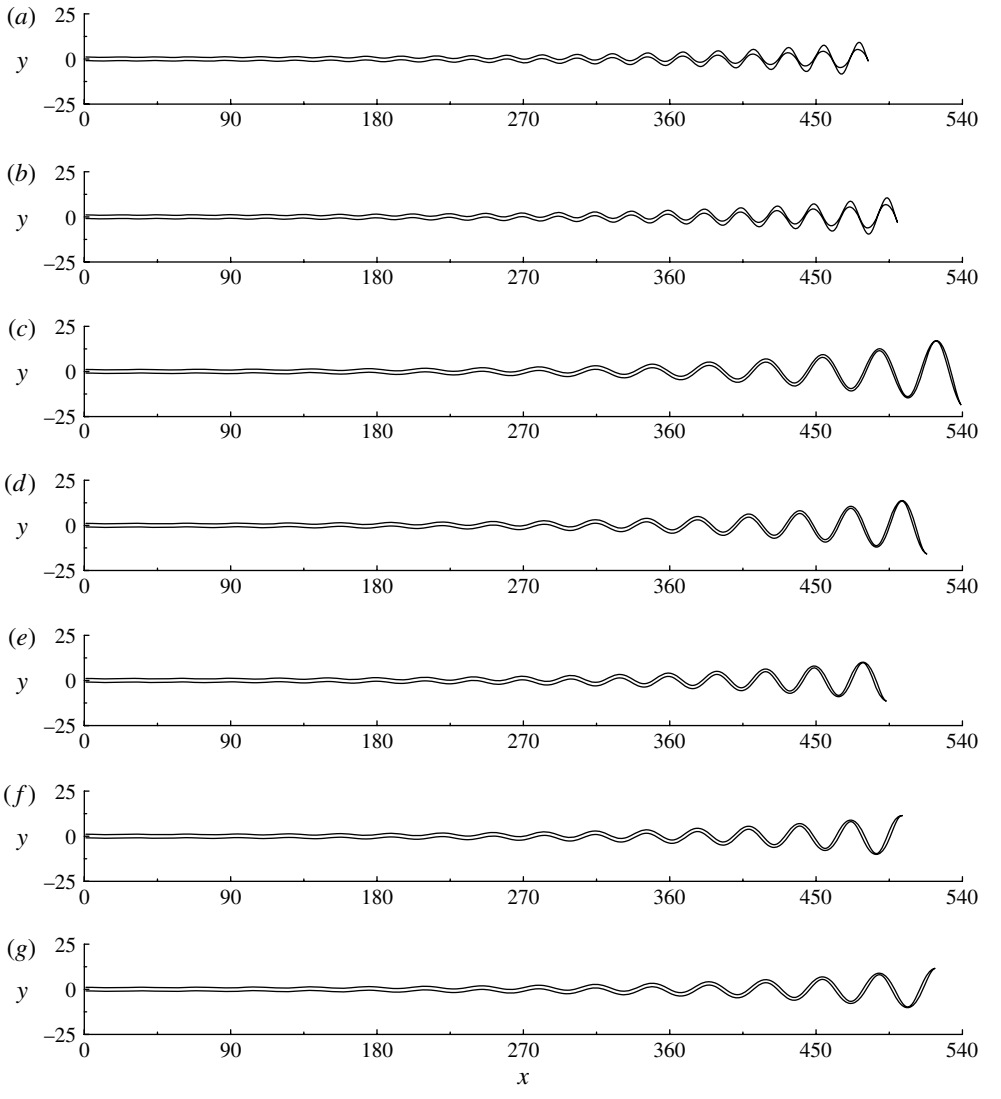


FIGURE 19. Spatial evolution of interface deformation for different Reynolds numbers at $We = 400$, $\rho = 0.001$: (*a*) $Re = \infty$, $k_1 = 0.29 - 0.0090\mathrm{i}$, $l_d = 482$; (*b*) $Re = 500$, $k_1 = 0.28 - 0.0090\mathrm{i}$, $l_d = 500$; (*c*) $Re = 150$, $k_1 = 0.18 - 0.0098\mathrm{i}$, $l_d = 539$; (*d*) $Re = 50$, $k_1 = 0.20 - 0.0098\mathrm{i}$, $l_d = 518$; (*e*) $Re = 10$, $k_1 = 0.21 - 0.0096\mathrm{i}$, $l_d = 493$; (*f*) $Re = 3$, $k_1 = 0.20 - 0.0094\mathrm{i}$, $l_d = 502$; (*g*) $Re = 1$, $k_1 = 0.18 - 0.0091\mathrm{i}$, $l_d = 523$.

unstable a flow which is stable for an inviscid fluid; it may also make a flow for an inviscid fluid more unstable.

In the situation described above, the complicated dual role played by viscosity may be attributed to two aspects: on one hand, it has a damping effect by dissipating energy, as has been shown that the temporal growth rate decreases with the decrease of Reynolds numbers; on the other hand, viscosity changes the property and condition of the disturbances, corresponding to the complicated variation of the second-order disturbance amplitude with different Reynolds numbers. Many authors have tried to explain the destabilizing effect of viscosity. Prandtl (1935) and Drazin (2002)

https://doi.org/10.1017/jfm.2013.502 Published online by Cambridge University Press

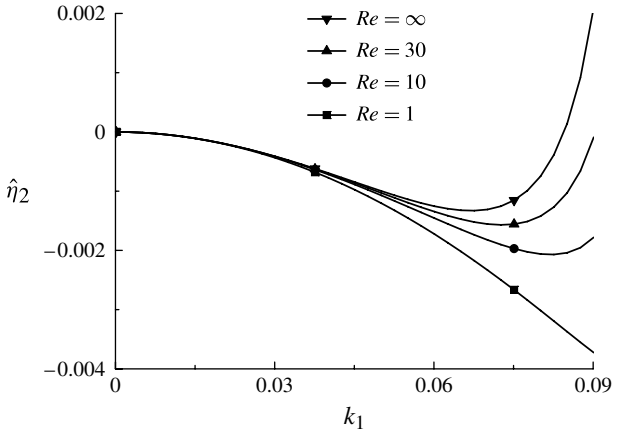


FIGURE 20. The initial amplitude of second-order interface disturbance at $We = 100$, $\rho = 0.001$.

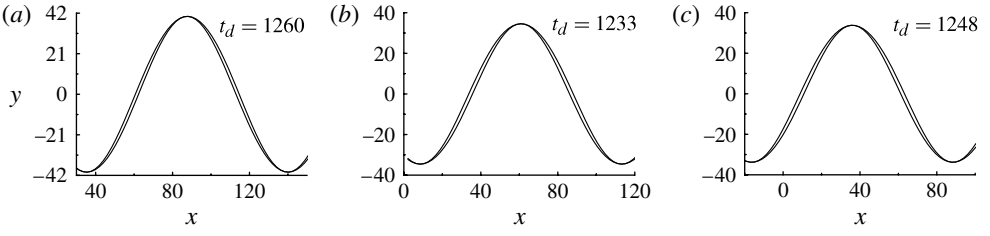


FIGURE 21. The shape of interface deformation at breakup time for different Reynolds numbers at $We = 100$, $\rho = 0.001$, $k = 0.06$: (*a*) $Re = \infty$, $t_d = 1260$; (*b*) $Re = 1$, $t_d = 1233$; (*c*) $Re = 0.1$, $t_d = 1248$.

attributed it to the energy transfer from the basic flow to the perturbation by means of Reynolds stress, and Taylor (1915) suggested that for the wall boundary, the viscosity's prevention of slip at the walls might permit generation of a perturbation momentum, which causes the instability.

Generally, under the normal conditions examined in this paper, the effect of viscosity on sheet instability is much weaker than that of gas-to-liquid density ratio and Weber number, because the variation of breakup time or length is very limited over the large variation of Reynolds numbers. A similar conclusion was drawn by Cousin & Dumouchel (1996), who proved that for planar sheets, the effect of viscosity can be neglected for a wide range of parameters. Since the Weber number and the gas-to-liquid density ratio are the predominant parameters, the wave instability of the liquid sheets is caused mainly by aerodynamic interaction with the surrounding gas.

The weak effect of viscosity may be difficult to observe through experimentation. Arai & Hashimoto (1986), Negeed *et al.* (2011) and Mouis (2003) have conducted experiments on planar sheets. Very different empirical equations have been developed from the intact length data as a function of sheet thickness, Reynolds number, and Weber number. The effect of Reynolds number also varies considerably from one to another. However, the liquid used in their experiments was simply water;

https://doi.org/10.1017/jfm.2013.502 Published online by Cambridge University Press

the effect of the liquid property was not considered. The Ohnesorge number, $Z = \mu/\sqrt{\rho_l a\sigma} = \sqrt{We}/Re$, of their experimental data is a fixed value; the Reynolds number and the Weber number have a fixed relation at different velocities. Therefore the correlations they obtained may not be sufficient to explain the effect of changing the Reynolds number at a constant Weber number, which is investigated in this paper. Heislbetz *et al.* (2007) conducted experiments on the liquid sheets formed by a doublet impinging jet. Results showed that a sheet with high viscosity is far more stable than a low-viscosity sheet at the same jet velocity. But this is not caused by the effect of viscosity on the instability of liquid sheet, since in their study the temporal growth rate is nearly the same for high-viscosity and low-viscosity sheets. The real reason seems to be the difference in geometric character: the thickness of a high-viscosity sheet is much greater than that of a low-viscosity sheet, and this gives the high-viscosity sheet a much greater dimensional breakup length. So this does not contradict the present study.

The last situation to be briefly discussed is the viscosity-enhanced instability in linear temporal instability presented by Li & Tankin (1991). This happens only for very small Weber numbers and Reynolds numbers and very large gas-to-liquid density ratios. When the Weber number is larger than 1.6, or the gas-to-liquid density ratio is smaller than 0.05, this phenomenon disappears. The dispersion relation is shown in figure 22. There are two unstable regions: the region corresponding to smaller wavenumbers is called 'aerodynamic instability' and the region with a much larger wave range is called 'viscosity-enhanced instability' by Li & Tankin (1991). The inviscid sheets have only aerodynamic instability, and the temporal growth rate for aerodynamic instability remains nearly the same for all Reynolds numbers. The temporal growth rate for viscosity-enhanced instability increases with the decrease of Reynolds number, so the viscosity has a destabilizing effect according to linear analysis. The interface deformations at breakup time for two typical situations are shown in figure 23. The wave deformations for these two cases are very similar. According to the breakup time, it can be concluded that viscosity does enhance instability under this condition. However, the temporal growth rate is too small and the breakup time is too long compared to the cases previously discussed, so this instability is too weak. Considering the rare conditions needed, this 'viscosity-enhanced' instability may be too difficult to observe.

Finally, we remark on the extent of nonlinearity in the cases studied in this paper. Although the disturbance amplitudes become very large, they are caused by large amplitudes of the first-order linear disturbances; the second-order nonlinear amplitudes only take a very small proportion. For the perturbation solution in this paper, the disturbance amplitude η_a can be expressed as

$$\eta_a = \eta_{a1} + \eta_{a2} + \eta_{a3} + \cdots, \tag{4.2}$$

where η_{a1}, η_{a2}, and η_{a3} are the disturbance amplitudes of the first, second and third order respectively. Take figures 7(*a*), 7(*b*) and 7(*c*) for example: at breakup time, the values of η_{a2}/η_{a1} are 0.039, 0.12 and 0.27 respectively, and 0.27 in figure 7(*c*) is actually the largest value of all the figures in this paper. Therefore, the nonlinearity is very weak. This can also be confirmed by the fact that the linear sinuous character is prominent in all figures showing the wave profile. It is assumed that this trend goes to higher orders, i.e. η_{a3}/η_{a2}, η_{a4}/η_{a3}, ... have parallel values as η_{a2}/η_{a1}, and in this way, the disturbance amplitudes of higher orders are very small and negligible. To ensure the small value of η_{a2}/η_{a1}, it is recommended that the present theory be applied in situations where $\rho We < 1$. Because we have not solved the solutions of higher-order

https://doi.org/10.1017/jfm.2013.502 Published online by Cambridge University Press

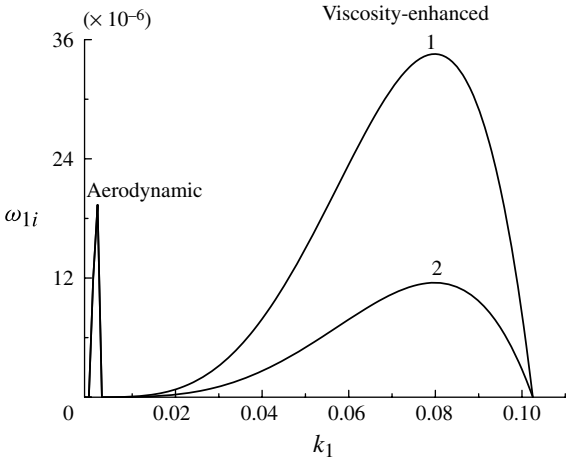


FIGURE 22. Dispersion relation for viscosity-enhanced instability at $We = 1.025$, $\rho = 0.1$: curve 1, $Re = 0.1$; curve 2, $Re = 0.3$.

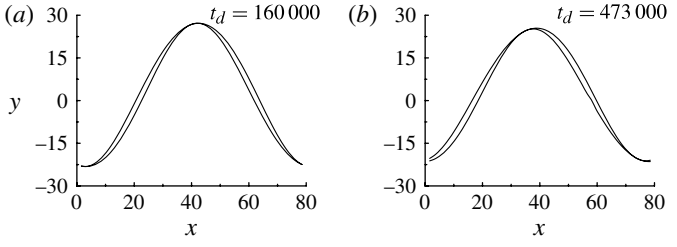


FIGURE 23. The shape of surface deformation at breakup time for viscosity-enhanced instability at $k_1 = 0.08$, $We = 1.025$, $\rho = 0.1$, (*a*) $Re = 0.1$, $\hat{\eta}_{j21}/\hat{\eta}_{j1}^2 = -3.20 \times 10^{-3} - 6.72 \times 10^{-4}$i, $t_d = 160\,000$; (*b*) $Re = 0.3$, $\hat{\eta}_{j21}/\hat{\eta}_{j1}^2 = -3.22 \times 10^{-3} - 2.02 \times 10^{-3}$i, $t_d = 473\,000$.

disturbances, we cannot estimate the errors caused by neglecting the higher-order terms, nor can we assert that the disturbance amplitudes of higher orders are certain to be very small and negligible. This is a limitation of the present study. The influence of higher-order harmonics will be left for further research.

5. Conclusions

A weakly nonlinear instability of two-dimensional planar viscous sheets moving in an inviscid and incompressible gas medium has been investigated using a perturbation technique. The second-order governing equations and interface disturbance solutions of the linear sinuous mode for both temporal and spatial instability have been derived. It is found that the second-order disturbance of the fundamental sinuous wave is varicose or dilational, causing disintegration and resulting in ligaments which are interspaced by half a wavelength. The breakup time for temporal instability and the breakup length for spatial instability have been calculated to estimate the extent of the instability. The interface deformations have been shown. The conclusions obtained from the temporal and spatial instability are generally identical. The effect of the Weber number, gas-to-

https://doi.org/10.1017/jfm.2013.502 Published online by Cambridge University Press

liquid density ratio and Reynolds number have been discussed. Results indicate that for a wide range of parameters, shorter waves have stronger nonlinear initial amplitude, and the most unstable wavenumber predicted by nonlinear analysis is slightly larger than linear analysis. The first-order growth rate and the second-order initial amplitude work together to cause the breakup. Increasing the Weber number and the gas-to-liquid density ratio will increase both the first-order growth rate and the second-order initial amplitude extensively, resulting in a much shorter breakup time or length, and a more distorted interface deformation. When the Weber number or the gas-to-liquid density ratio is very small, it takes a rather long time to disintegrate and the sheet is approximately stable. Under normal conditions, viscosity has a stabilizing effect on the first-order temporal or spatial growth rate, but it plays a dual role on the second-order disturbance amplitude. The overall effect of viscosity assessed by the breakup time or length is minor and complicated. For most of the common conditions, viscosity reduces instability at large or small Reynolds numbers, but enhances instability at medium Reynolds numbers. At the typical condition of $We = 400$ and $\rho = 0.001$, viscosity has a weak stabilizing effect when the Reynolds number is larger than 150 or smaller than 10 and a weak destabilizing effect when the Reynolds number is between 150 and 10. The viscosity-enhanced instability under very small Weber numbers and very large gas-to-liquid density ratios has also been examined; the conclusion reached is the same as in the linear analysis.

Acknowledgement

Acknowledgements are made to China's National Nature Science Funds for financial support (support no. 11272036 and 51078014).

Appendix A. Disturbance amplitude in temporal instability

$$\hat{f}_\eta = (-2B_1 l_1 \sinh l_1 y - 2D_1 k_1 \sinh k_1 y)\,\hat{\eta}_{j1}, \tag{A 1}$$

$$\hat{f}_\mu = \left[\frac{l_1}{k_1}(l_1^2 + 5k_1^2)\mathrm{i}B_1 \sinh l_1 y + 6\mathrm{i}k_1^2 D_1 \sinh k_1 y\right]\hat{\eta}_{j1}, \tag{A 2}$$

$$\hat{f}_d = \left(\frac{4l_1^2 + 2k_1^2}{Re}B_1 \cosh l_1 y + \frac{l_1^2 + 5k_1^2}{Re}D_1 \cosh k_1 y\right)\hat{\eta}_{j1} + \hat{\eta}_{j1}^2 \rho\omega_1^2 \exp[k_1 + (-1)^j k_1 y], \tag{A 3}$$

$$\hat{f}_u = \frac{\mathrm{i}}{2k_1}\left(\hat{f}_p + \frac{\mathrm{d}\hat{f}_v}{\mathrm{d}y}\right), \tag{A 4}$$

$$\hat{f}_v = 0, \tag{A 5}$$

$$\hat{f}_p = 2(l_1^2 B_1^2 + k_1^2 D_1^2) + (l_1 - k_1)^2 B_1 D_1 \cosh(l_1 y + k_1 y) + (l_1 + k_1)^2 B_1 D_1 \cosh(l_1 y - k_1 y), \tag{A 6}$$

$$\hat{h}_u = \frac{\mathrm{i}}{2k_1}\frac{\mathrm{d}\hat{h}_v}{\mathrm{d}y}, \tag{A 7}$$

$$\hat{h}_v = ReB_1 D_1 (l_1^2 - k_1^2) \times \left\{\frac{\sinh(l_1 y + k_1 y)}{(l_1 + 3k_1)\left[(l_1 + k_1)^2 - l_{21}^2\right]} + \frac{\sinh(l_1 y - k_1 y)}{(l_1 - 3k_1)\left[(l_1 - k_1)^2 - l_{21}^2\right]}\right\}, \tag{A 8}$$

https://doi.org/10.1017/jfm.2013.502 Published online by Cambridge University Press

$$\hat{h}_p = -\frac{1}{2k_1^2}(l_1^2B_1^2 + k_1^2D_1^2) + \frac{l_1 - k_1}{l_1 + 3k_1}B_1D_1\cosh(l_1y + k_1y) + \frac{l_1 + k_1}{l_1 - 3k_1}B_1D_1\cosh(l_1y - k_1y), \tag{A 9}$$

where B_1, D_1, and l_1 are defined in (3.5).

Appendix B. Disturbance amplitude in spatial instability

$$\hat{\eta}'_{j21} = -(-1)^j\left\{\frac{(l_{21}^2 + 4k_1^2)\coth 2k_1}{2Rek_1(4k_1^2 - l_{21}^2)}\left[Re\left(\frac{\mathrm{d}\hat{h}_p}{\mathrm{d}y} + \hat{f}_v\right) - 2\mathrm{i}k_1\hat{f}_\mu + (4k_1^2 + l_{21}^2)\hat{f}_\eta\right] + \frac{4\mathrm{i}k_1l_{21}\coth l_{21}}{Re(4k_1^2 - l_{21}^2)}\left[\frac{\mathrm{i}}{2k_1}Re\left(\frac{\mathrm{d}\hat{h}_p}{\mathrm{d}y} + \hat{f}_v\right) + \hat{f}_\mu + 4\mathrm{i}k_1\hat{f}_\eta - \frac{\mathrm{i}(4k_1^2 - l_{21}^2)}{2k_1}\hat{h}_v\right] + \hat{h}_p - \frac{2}{Re}\frac{\mathrm{d}\hat{h}_v}{\mathrm{d}y} + 2\rho\omega_1^2\hat{\eta}_{j1}^2 - \hat{f}_d\right\}\Bigg|_{y=1}\frac{2k_1}{D_{var}(2\omega_1, 2k_1)}, \tag{B 1}$$

$$\hat{\eta}'_{j22} = (-1)^{j+1}\left\{\frac{(l_{22}'^2 - 4k_{1i}^2)\coth 2\mathrm{i}k_{1i}}{2\mathrm{i}Rek_{1i}(-4k_{1i}^2 - l_{22}'^2)}\left[Re\left(\frac{\mathrm{d}\hat{j}'_p}{\mathrm{d}y} + \hat{g}'_v\right) + 2k_{1i}\hat{g}'_\mu + (l_{22}'^2 - 4k_{1i}^2)\hat{g}'_\eta\right] + \frac{-4k_{1i}l'_{22}\coth l'_{22}}{Re(-4k_{1i}^2 - l_{22}'^2)}\left[\frac{1}{2k_{1i}}Re\left(\frac{\mathrm{d}\hat{j}'_p}{\mathrm{d}y} + \hat{g}'_v\right) + \hat{g}'_\mu - 4k_{1i}\hat{g}'_\eta - \frac{(-4k_{1i}^2 - l_{22}'^2)}{2k_{1i}}\hat{j}'_v\right] + \hat{j}'_p - \frac{2}{Re}\frac{\mathrm{d}\hat{j}'_v}{\mathrm{d}y} + \rho\omega_1^2\hat{\eta}_{j1}\overline{\hat{\eta}}_{j1} - \hat{g}'_d\right\}\Bigg|_{y=1}\frac{2\mathrm{i}k_{1i}}{D_{var}(0, 2\mathrm{i}k_{1i})}, \tag{B 2}$$

$$l_{22}'^2 = -4k_{1i}^2 - 2Rek_{1i}, \tag{B 3}$$

$$\hat{g}'_v = \frac{B_1\overline{B}_1}{2k_1\overline{k}_1}k_{1r}\left(\overline{k}_1l_1 + k_1\overline{l}_1\right)\sinh\left(l_1y + \overline{l}_1y\right) + \frac{B_1\overline{B}_1}{2k_1\overline{k}_1}k_{1r}\left(\overline{k}_1l_1 - k_1\overline{l}_1\right) \times \sinh\left(l_1y - \overline{l}_1y\right) + \frac{k_1 + \overline{k}_1}{2k_1}B_1\overline{D}_1\left(k_1 + l_1\right)\sinh\left(l_1y + \overline{k}_1y\right) + \frac{k_1 + \overline{k}_1}{2k_1}B_1\overline{D}_1\left(l_1 - k_1\right)\sinh\left(l_1y - \overline{k}_1y\right) + \frac{\left(k_1 + \overline{k}_1\right)}{2}D_1\overline{D}_1\sinh\left(k_1y + \overline{k}_1y\right), \tag{B 4}$$

$$\hat{g}'_\mu = \left[\frac{l_1}{k_1}(l_1^2 + k_1^2 - 4k_1\overline{k}_1)\mathrm{i}B_1\sinh l_1y + \mathrm{i}k_1D_1(2k_1 - 4\overline{k}_1)\sinh k_1y\right]\overline{\hat{\eta}}_{j1}, \tag{B 5}$$

$$\hat{g}'_\eta = \frac{\overline{k}_1 - k_1}{k_1}\left[l_1B_1\sinh l_1y + k_1D_1\sinh k_1y\right]\overline{\hat{\eta}}_{j1}, \tag{B 6}$$

$$\hat{g}'_d = \left[\frac{2}{Re}B_1\left(l_1^2 - \frac{l_1^2\overline{k}_1}{k_1} - k_1\overline{k}_1\right)\cosh l_1y + \frac{1}{Re}D_1\left(l_1^2 + k_1^2 - 4k_1\overline{k}_1\right)\cosh k_1y\right]\overline{\hat{\eta}}_{j1} + \hat{\eta}_{j1}\overline{\hat{\eta}}_{j1}\rho\omega_1^2\exp[k_1 + (-1)^jk_1y], \tag{B 7}$$

https://doi.org/10.1017/jfm.2013.502 Published online by Cambridge University Press

$$\hat{j}_v' = \frac{B_1\overline{B}_1 Re}{2k_1\bar{k}_1\left[\left(l_1+\bar{l}_1\right)^2 - l_{22}'^2\right]}\left[k_{1r}(\bar{k}_1 l_1 + k_1\bar{l}_1) - \frac{\left(\bar{k}_1 l_1 + k_1\bar{l}_1\right)^2(l_1+\bar{l}_1)}{\left(l_1+\bar{l}_1\right)^2 + 4k_{1i}^2}\right]$$
$$\times \sinh(l_1 y + \bar{l}_1 y) + \frac{B_1\overline{B}_1 Re}{2k_1\bar{k}_1\left[\left(l_1-\bar{l}_1\right)^2 - l_{22}'^2\right]}$$
$$\times \left[k_{1r}(\bar{k}_1 l_1 - k_1\bar{l}_1) - \frac{\left(\bar{k}_1 l_1 - k_1\bar{l}_1\right)^2(l_1-\bar{l}_1)}{\left(l_1-\bar{l}_1\right)^2 + 4k_{1i}^2}\right]$$
$$\times \sinh(l_1 y - \bar{l}_1 y) + \frac{B_1\overline{D}_1 Re}{k_1\left[\left(l_1+\bar{k}_1\right)^2 - l_{22}'^2\right]}$$
$$\times \left[k_{1r}(k_1+l_1) - \bar{k}_1\frac{(l_1+k_1)^2(l_1+\bar{k}_1)}{\left(l_1+\bar{k}_1\right)^2 + 4k_{1i}^2}\right]$$
$$\times \sinh(l_1 y + \bar{k}_1 y) + \frac{B_1\overline{D}_1 Re}{k_1\left[\left(l_1-\bar{k}_1\right)^2 - l_{22}'^2\right]}$$
$$\times \left[k_{1r}(l_1-k_1) - \bar{k}_1\frac{(l_1-k_1)^2(l_1-\bar{k}_1)}{\left(l_1-\bar{k}_1\right)^2 + 4k_{1i}^2}\right]$$
$$\times \sinh(l_1 y - \bar{k}_1 y) + \frac{\left(k_1+\bar{k}_1\right)D_1\overline{D}_1 Re}{\left(k_1+\bar{k}_1\right)^2 - l_{22}'^2}$$
$$\times \left[\frac{1}{2} - \frac{2k_1\bar{k}_1}{\left(k_1+\bar{k}_1\right)^2 + 4k_{1i}^2}\right]\sinh\left(k_1 y + \bar{k}_1 y\right), \tag{B 8}$$

$$\hat{j}_p' = -\frac{B_1\overline{B}_1}{2k_1\bar{k}_1}\frac{\left(\bar{k}_1 l_1 + k_1\bar{l}_1\right)^2}{\left(l_1+\bar{l}_1\right)^2 + 4k_{1i}^2}\cosh\left(l_1 y + \bar{l}_1 y\right)$$
$$- \frac{B_1\overline{B}_1}{2k_1\bar{k}_1}\frac{\left(\bar{k}_1 l_1 - k_1\bar{l}_1\right)^2}{\left(l_1-\bar{l}_1\right)^2 + 4k_{1i}^2}\cosh\left(l_1 y - \bar{l}_1 y\right)$$
$$- \frac{B_1\overline{D}_1\bar{k}_1(k_1+l_1)^2}{k_1\left[\left(\bar{k}_1+l_1\right)^2 + 4k_{1i}^2\right]}\cosh\left(l_1 y + \bar{k}_1 y\right)$$
$$- \frac{B_1\overline{D}_1\bar{k}_1(k_1-l_1)^2}{k_1\left[\left(\bar{k}_1-l_1\right)^2 + 4k_{1i}^2\right]}\cosh\left(l_1 y - \bar{k}_1 y\right)$$
$$- \frac{2k_1\bar{k}_1 D_1\overline{D}_1}{\left(\bar{k}_1+k_1\right)^2 + 4k_{1i}^2}\cosh\left(k_1 y + \bar{k}_1 y\right). \tag{B 9}$$

Appendix C. Dynamic boundary condition for inviscid sheets

The dynamic boundary conditions for inviscid sheets vary in the studies of different authors, so we revisit this problem and prove our opinion.

If the flow field of the inviscid sheet is initially irrotational, it has a velocity potential defined as ϕ. The relation between velocity and the velocity potential is

$$\boldsymbol{v} = \nabla\phi, \quad \boldsymbol{v}_g = \nabla\phi_g. \tag{C 1}$$

https://doi.org/10.1017/jfm.2013.502 Published online by Cambridge University Press

Note that ϕ contains the basic x direction uniform flow, i.e. for undisturbed flow, $\phi = x$. The normal stress on the interface should be continuous, so the dynamic boundary condition requires

$$\frac{1}{2} + \rho\frac{\partial\phi_{gj}}{\partial t} - \frac{\partial\phi}{\partial t} + \frac{1}{2}\rho\left[\left(\frac{\partial\phi_{gj}}{\partial x}\right)^2 + \left(\frac{\partial\phi_{gj}}{\partial y}\right)^2\right] - \frac{1}{2}\left[\left(\frac{\partial\phi}{\partial x}\right)^2 + \left(\frac{\partial\phi}{\partial y}\right)^2\right]$$
$$= \frac{(-1)^j}{We}\frac{\dfrac{\partial^2\eta_j}{\partial x^2}}{\left[1 + \left(\dfrac{\partial\eta_j}{\partial x}\right)^2\right]^{3/2}} \quad \text{at } y = (-1)^{j+1} + \eta_j, \tag{C 2}$$

where the pressure has been indicated using Cauchy–Lagrange integration:

$$p_{gj} = -\rho\left[\frac{\partial\phi_{gj}}{\partial t} + \frac{1}{2}\left(\frac{\partial\phi_{gj}}{\partial x}\right)^2 + \frac{1}{2}\left(\frac{\partial\phi_{gj}}{\partial y}\right)^2\right], \tag{C 3a}$$

$$p = -\left[\frac{\partial\phi}{\partial t} + \frac{1}{2}\left(\frac{\partial\phi}{\partial x}\right)^2 + \frac{1}{2}\left(\frac{\partial\phi}{\partial y}\right)^2\right] + \frac{1}{2}. \tag{C 3b}$$

The term $\frac{1}{2}$ in the second equation is the integration constant making the basic flow pressure zero. As it does not appear in the boundary condition of Clark & Dombrowski (1972), their boundary condition for basic flow does not hold.

Using the perturbation technique (which is the same as in § 2), the first-order and second-order boundary condition can be derived:

$$\rho\frac{\partial\phi_{gj1}}{\partial t} - \frac{\partial\phi_1}{\partial t} - \frac{\partial\phi_1}{\partial x} - \frac{(-1)^j}{We}\frac{\partial^2\eta_{j1}}{\partial x^2} = 0 \quad \text{at } y = (-1)^{j+1}, \tag{C 4}$$

$$\rho\frac{\partial\phi_{gj2}}{\partial t} - \frac{\partial\phi_2}{\partial t} - \frac{\partial\phi_2}{\partial x} - \frac{(-1)^j}{We}\frac{\partial^2\eta_{j2}}{\partial x^2} = \eta_{j1}\left(-\rho\frac{\partial^2\phi_{gj1}}{\partial t\partial y} + \frac{\partial^2\phi_1}{\partial t\partial y} + \frac{\partial^2\phi_1}{\partial x\partial y}\right)$$
$$-\frac{\rho}{2}\left[\left(\frac{\partial\phi_{gj1}}{\partial x}\right)^2 + \left(\frac{\partial\phi_{gj1}}{\partial y}\right)^2\right] + \frac{1}{2}\left[\left(\frac{\partial\phi_1}{\partial x}\right)^2 + \left(\frac{\partial\phi_1}{\partial y}\right)^2\right] \quad \text{at } y = (-1)^{j+1} \tag{C 5}$$

where (C 5) is identical to (2.31) when $Re \to \infty$.

The non-dimensionalized second-order equation of Clark & Dombrowski (1972) is

$$\frac{\partial\phi_2}{\partial t} - \rho\frac{\partial\phi_{gj2}}{\partial t} - \frac{1}{2}\left[\left(\frac{\partial\phi_1}{\partial x}\right)^2 + \left(\frac{\partial\phi_1}{\partial y}\right)^2 + 2\frac{\partial\phi_0}{\partial x}\frac{\partial\phi_2}{\partial x}\right] + \frac{\rho}{2}\left[\left(\frac{\partial\phi_{gj1}}{\partial x}\right)^2 + \left(\frac{\partial\phi_{gj1}}{\partial y}\right)^2\right]$$
$$-\eta_{j1}\left(\rho\frac{\partial^2\phi_{gj1}}{\partial t\partial y} + \frac{\partial^2\phi_1}{\partial t\partial y} - \frac{\partial\phi_0}{\partial x}\frac{\partial^2\phi_1}{\partial x\partial y}\right) = \frac{(-1)^j}{We}\frac{\partial^2\eta_{j2}}{\partial x^2} \quad \text{at } y = (-1)^{j+1} \tag{C 6}$$

where ϕ_1, ϕ_2, ϕ_{gj1}, ϕ_{gj2}, η_{j1} and η_{j2} in (C 6) correspond to non-dimensionalized ${}^1\phi$, ${}^2\phi$, ${}^1\phi_j'$, ${}^2\phi_j'$, ${}^1\eta_j$ and ${}^2\eta_j$ in the study of Clark & Dombrowski (1972). The velocity potential they defined is the opposite of the definition in this paper:

$$\boldsymbol{v} = -\nabla\phi, \quad \boldsymbol{v}_g = -\nabla\phi_g. \tag{C 7}$$

The zero-order velocity potential identifying the basic flow is

$$\phi_0 = -x. \tag{C 8}$$

https://doi.org/10.1017/jfm.2013.502 Published online by Cambridge University Press

Despite the definition of velocity potential, there is a small difference between (C 5) and (C 6), for if we replace every velocity potential with its opposite number in (C 6), the signs of the terms '$\eta_{j1}\left(\partial^2\phi_1/\partial t\partial y\right)$' and '$\eta_{j1}\left(\partial\phi_0/\partial x\right)\left(\partial^2\phi_1/\partial x\partial y\right)$' in (C 6) are opposite to those in (C 5). We believe this is a typographical omission by the authors.

The second-order dynamic boundary condition presented by Jazayeri & Li (2000) is

$$\rho\frac{\partial\phi_{gj2}}{\partial t}-\frac{\partial\phi_2}{\partial t}-\frac{\partial\phi_2}{\partial x}-\frac{(-1)^j}{We}\frac{\partial^2\eta_{j2}}{\partial x^2}=-\rho\left(\frac{\partial\eta_{j1}}{\partial t}\frac{\partial\phi_{gj1}}{\partial y}+\eta_{j1}\frac{\partial^2\phi_{gj1}}{\partial y\partial t}\right)$$
$$+\left(\frac{\partial\eta_{j1}}{\partial t}\frac{\partial\phi_1}{\partial y}+\eta_{j1}\frac{\partial^2\phi_1}{\partial y\partial t}\right)-\frac{1}{2}\rho\left[\left(\frac{\partial\phi_{gj1}}{\partial x}\right)^2+\left(\frac{\partial\phi_{gj1}}{\partial y}\right)^2\right]$$
$$+\frac{1}{2}\left[\left(\frac{\partial\phi_1}{\partial x}\right)^2+\left(\frac{\partial\phi_1}{\partial y}\right)^2\right]+\left(\frac{\partial\eta_{j1}}{\partial x}\frac{\partial\phi_1}{\partial y}+\eta_{j1}\frac{\partial^2\phi_1}{\partial y\partial x}\right)\quad\text{at } y=(-1)^{j+1},\quad\text{(C 9)}$$

where ϕ_1, ϕ_2, ϕ_{gj1}, ϕ_{gj2}, η_{j1} and η_{j2} in (C 9) correspond to ϕ_{l1}, ϕ_{l2}, ϕ_{g1}, ϕ_{g2}, η_{j1} and η_{j2} in the study of Jazayeri & Li (2000). The sign of every term in (C 5) is identical to that of (C 9). However, compared to (C 9), (C 5) does not have the terms '$-\rho\left(\partial\eta_{j1}/\partial t\right)\left(\partial\phi_{gj1}/\partial y\right)$', '$\left(\partial\eta_{j1}/\partial t\right)\left(\partial\phi_1/\partial y\right)$' and '$\left(\partial\eta_{j1}/\partial x\right)\left(\partial\phi_1/\partial y\right)$'. This is because they did not use the technique shown in (2.13) to expand

$$\left.\frac{\partial\phi}{\partial x}\right|_{y=(-1)^{j+1}+\eta_j},\quad\left.\frac{\partial\phi}{\partial t}\right|_{y=(-1)^{j+1}+\eta_j}\quad\text{and}\quad\left.\frac{\partial\phi_{gj}}{\partial t}\right|_{y=(-1)^{j+1}+\eta_j},\qquad\text{(C 10)}$$

which are required in (C 2). Instead, they expanded

$$\left.\phi\right|_{y=(-1)^{j+1}+\eta_j}\quad\text{and}\quad\left.\phi_{gj}\right|_{y=(-1)^{j+1}+\eta_j}\qquad\text{(C 11)}$$

and obtained

$$\frac{\partial\left(\left.\phi\right|_{y=(-1)^{j+1}+\eta_j}\right)}{\partial x},\quad\frac{\partial\left(\left.\phi\right|_{y=(-1)^{j+1}+\eta_j}\right)}{\partial t}\quad\text{and}\quad\frac{\partial\left(\left.\phi_{gj}\right|_{y=(-1)^{j+1}+\eta_j}\right)}{\partial t}.\qquad\text{(C 12)}$$

Because η_j is a function of x and t, the terms in (C 12) are not identical to those in (C 10). Therefore, this method does not appear to be appropriate.

REFERENCES

ARAI, T. & HASHIMOTO, H. 1986 Disintegration of a thin liquid sheet in a concurrent gas stream. *Intl J. Turbo Jet Engines* **3**, 301–306.

ASARE, H. R., TAKAHASHI, R. K. & HOFFMAN, M. A. D. 1981 Liquid sheet jet experiments: comparison with linear theory. *Trans. ASME: J. Fluids Engng* **103**, 595–604.

CAO, J. & LI, X. 2000 Stability of plane liquid sheets in compressible gas streams. *AIAA J. Propulsion Power* **16**, 623–627.

CHANDRASEKHAR, C. 1961 *Hydrodynamic and Hydromagnetic Stability*. Oxford University Press.

CLARK, C. J. & DOMBROWSKI, N. 1972 Aerodynamic instability and disintegration of inviscid liquid sheets. *Proc. R. Soc. Lond.* A **329**, 467–478.

COUSIN, J. & DUMOUCHEL, C. 1996 The effect of viscosity on the linear instability of a flat liquid sheet. *Atomiz. Sprays* **6**, 563–576.

CRAPPER, G. D., DOMBROWSKI, N. & PYOTT, G. A. D. 1975 Large amplitude Kelvin–Helmholtz waves on thin liquid sheets. *Proc. R. Soc. Lond.* A **342**, 209–224.

DE WIT, A., GALLEZ, D. & CHRISTOV, C. I. 1994 Nonlinear evolution equations for thin liquid films with insoluble surfactants. *Phys. Fluids* **6**, 3256–3266.

https://doi.org/10.1017/jfm.2013.502 Published online by Cambridge University Press

DOMBROWSKI, N. & JOHNS, W. R. 1963 The aerodynamic instability and disintegration of viscous liquid sheets. *Chem. Engng Sci.* **18**, 203–214.

DRAZIN, P. G. 2002 Stability characteristics of some flows of a viscous fluid. In *Introduction to Hydrodynamic Stability*. Cambridge University Press.

ERNEUX, T. & DAVIS, S. H. 1993 Nonlinear rupture of free films. *Phys. Fluids* A **5**, 1117–1122.

FRASER, R. P. & EISENKLAM, P. 1953 Research into the performance of atomizers of liquids. *Imp. Colloid Chem. Engng Soc. J.* **7**, 52–68.

GASTER, M. 1962 A note on the relation between temporally-increasing and spatially-increasing disturbances in hydrodynamic stability. *J. Fluid Mech.* **14**, 222–224.

HAGERTY, W. W. & SHEA, J. F. 1955 A study of the stability of plane fluid sheets. *J. Appl. Mech.* **22**, 509–514.

HEISENBERG, W. 1924 Über Stabilität und Turbulenz von Flüssigkeitsströmen. *Ann. Phys.* **74**, 577–627.

HEISLBETZ, B., MADLENER, K. & CIEZKI, H. K. 2007 Breakup characteristics of a Newtonian liquid sheet formed by a doublet impinging jet injector. In *43rd AIAA/ASME/SAE/ASEE Joint Propulsion Conference and Exhibit*, *AIAA Paper* 2007-5694.

HOGAN, S. J. 1986 Highest waves, phase speeds and particle trajectories of nonlinear capillary waves on sheets of fluid. *J. Fluid Mech.* **172**, 547–563.

HWANG, C. C., CHEN, J. L. & SHEN, L. F. 1996 Nonlinear rupture theory of a thin liquid films with insoluble surfactant. *J. Phys. Soc. Japan* **65**, 2494–2501.

IBRAHIM, A. A. & JOG, M. A. 2008 Nonlinear instability of an annular liquid sheet exposed to gas flow. *J. Multiphase Flow* **34**, 647–664.

JAZAYERI, S. A. & LI, X. 2000 Nonlinear instability of plane liquid sheets. *J. Fluid Mech.* **406**, 281–308.

KAN, K. & YOSHINAGA, T. 2007 Instability of a planar liquid sheet with surrounding fluids between two parallel walls. *Fluid Dyn. Res.* **39**, 389–412.

KINNERSLEY, W. 1976 Exact large amplitude capillary waves on sheets of fluid. *J. Fluid Mech.* **77**, 229–241.

LEE, D. S. 2002 Nonlinear instability of an electrohydrodynamic planar jet. *Z. Naturforsch.* A **57**, 682–688.

LI, H. S. & KELLY, R. E. 1992 The instability of a liquid jet in a compressible airstream. *Phys. Fluids* A **4**, 2162–2168.

LI, X. 1993 Spatial instability of plane liquid sheets. *Chem. Engng Sci.* **48**, 2973–2981.

LI, X. & TANKIN, R. S. 1991 On the temporal instability of a two-dimensional viscous liquid sheet. *J. Fluid Mech.* **226**, 425–443.

LIN, C. K., HWANG, C. C. & UEN, W. Y. 2000 A nonlinear rupture theory of thin liquid films with soluble surfactant. *J. Colloid Interface Sci.* **231**, 379–393.

LIN, S. P. 1981 Stability of a viscous liquid curtain. *J. Fluid Mech.* **104**, 111–118.

LIN, S. P., LIAN, Z. W. & CREIGHTON, B. J. 1990 Absolute and convective instability of a liquid sheet. *J. Fluid Mech.* **220**, 673–689.

MATSUUCHI, K. 1974 Modulational instability of nonlinear capillary waves on thin liquid sheet. *J. Phys. Soc. Japan* **37**, 1680–1687.

MATSUUCHI, K. 1976 Instability of thin liquid sheet and its break-up. *J. Phys. Soc. Japan* **41**, 1410–1416.

MEHRING, C. & SIRIGNANO, W. A. 1999 Nonlinear capillary wave distortion and disintegration of thin planar liquid sheets. *J. Fluid Mech.* **388**, 69–113.

MOUIS, A. G. 2003 Atomization processes of two-dimensional liquid sheets. PhD thesis, The Pennsylvania State University.

NEGEED, EL-SAYED R., HIDAKA, S., KOHNO, M. & TAKATA, Y. 2011 Experimental and analytical investigation of liquid sheet breakup characteristics. *Intl J. Heat Fluid Flow* **32**, 95–106.

PRANDTL, L. 1935 The mechanics of viscous fluids. In *Aerodynamic Theory,* vol. 3 (ed. W. F. Durand), pp. 34–208. Springer.

PRÉVOST, M. & GALLEZ, D. 1986 Nonlinear rupture of thin free liquid films. *J. Chem. Phys.* **84**, 4043–4048.

https://doi.org/10.1017/jfm.2013.502 Published online by Cambridge University Press

RANGEL, R. H. & SIRIGNANO, W. A. 1991 The linear and nonlinear shear instability of a fluid sheet. *Phys. Fluids* A **3**, 2392–2400.

RAYLEIGH, LORD 1879 On the instability of jets. *Proc. Lond. Math. Soc.* **10**, 4–13.

SCHLICHTING, H. 1933 Zur Entstehung der Turbulenz bei der Plattenströmung. *Nachr. Ges. Wiss. Göttingen*, 181–208.

SHARMA, A., KISHORE, C. S., SALANIWAL, S. & RUCKENSTEIN, E. 1995 Nonlinear stability and rupture of ultrathin free films. *Phys. Fluids* **7**, 1832–1840.

SIRIGNANO, W. A. & MEHRING, C. 2000 Review of theory of distortion and disintegration of liquid streams. *Prog. Energy Combust. Sci.* **26**, 609–655.

SQUIRE, H. B. 1953 Investigation of the instability of a moving liquid film. *Br. J. Appl. Phys.* **4**, 167–169.

TAMMISOLA, O., SASAKI, A., LUNDELL, F., MATSUBARA, M. & SÖDERBERG, L. D. 2011 Stabilizing effect of surrounding gas flow on a plane liquid sheet. *J. Fluid Mech.* **672**, 5–32.

TAYLOR, G. I. 1915 Eddy motion in the atmosphere. *Phil. Trans. R. Soc. Lond* A **215**, 1–26.

THARAKAN, T. J., RAMAMURTHI, K. & BALAKRISHNAN, M. 2002 Nonlinear breakup of thin liquid sheets. *Acta Mechanica* **156**, 29–46.

TOLLMIEN, W. 1929 Über die Entstehung der Turbulenz. *Nachr. Ges. Wiss. Göttingen*, 21–44.

VAYNBLAT, D., LISTER, J. R. & WITELSKI, T. P. 2001 Rupture of thin viscous films by van der Waals forces: evolution and self-similarity. *Phys. Fluids* **13**, 1130–1140.

YANG, L., FU, Q., QU, Y., GU, B. & ZHANG, M. 2012 Breakup of a power-law liquid sheet formed by an impinging jet injector. *Intl J. Multiphase Flow* **39**, 37–44.

YOSHINAGA, T. & KAN, K. 2006 Breakup of a falling liquid sheet caused by amplified modulational waves. *Fluid Dyn. Res.* **38**, 313–338.

YOSHINAGA, T. & UCHIYAMA, T. 2001 Behavior of a free liquid sheet subject to a temperature difference between both surfaces. *J. Phys. Soc. Japan* **70**, 103–110.

YOSHINAGA, T. & YOSHIDA, T. 2003 Nonlinear wave behaviour of the sinuous mode on a free liquid sheet with variable surface tension and viscosity. *J. Phys. Soc. Japan* **72**, 3113–3122.

https://doi.org/10.1017/jfm.2013.502 Published online by Cambridge University Press